Accepted Manuscript in Calphad - http://dx.doi.org/10.1016/j.calphad.2017.07.009

https://www.sciencedirect.com/science/article/pii/S0364591617300937

Ab initio-assisted assessment of the CaO-SiO_2 system under pressure

Donato Belmonte, Giulio Ottonello, Marino Vetuschi Zuccolini

DISTAV, Università di Genova, Corso Europa 26, 16132 Genova, Italy

1. Introduction

The substantial improvements in computing capability and the development of accurate computational codes render nowadays feasible the investigation of periodic structures by ab initio all-electron approaches. The adoption of appropriate Gaussian expansions, coupled with hybrid functionals, ensures that the static energy of the investigated crystals at the variational state plus zero-point and thermal corrections returns extremely accurate values of the absolute thermodynamic magnitudes which can be rapidly converted to the conventional ones by standard procedures [1]. The effect of thermal energy is appropriately accounted for by vibrational calculations and the ensuing parameterization in terms of heat capacity is so precise that a C_P=f(T) Shomate's function generated from ab-initio data can often be hardly recognizable from the best interpolant of calorimetric data of reference standard materials [2]. The mode-gamma analysis of the Hessian eigenvectors in the quasi-harmonic approximation is finally the main road toward an accurate account of the thermodynamic properties of any crystalline solid. All these procedures are nowadays routine. Concerning the substances that lack long-range periodicity, their abinitio characterization is still at an embryonic stage, but the observation that silicate liquids may be treated as polarized continua in the framework of Tomasi's Polarized Continuum Model [3] (and, as such, parameterized [4–6]) opens new perspectives toward a complete ab initio prediction of melting relations in chemically complex systems [7]. Having the various aggregation states of interest been resolved by first-principles, it follows that the magnitudes connected to the solid/ liquid state transition acquire new emphasis in the attempt to reconcile theory with observations. We present hereafter a first attempt toward an ab initio-assisted assessment of melting relations and sub-solidus phase equilibria in the system CaO-SiO_2. This system is prototypical in many aspects because the two limiting components have quite contrasting extrinsic stability limits in the crystalline state. The most refractory one (CaO) has the same cubic structure (B1) up to very high pressure [8,9], while extensive polymorphism is exhibited by silica (at least eight polymorphs of SiO_2 exist if one considers 2nd order transitions and disregards those on which there is poor consensus) [10,11]. The two components form also an orthosilicate and a metasilicate (as many other binary systems with SiO_2 as component) and all phases may be treated as purely stoichiometric

Table 1
Thermodynamic properties of the pure liquid components in the CaO-SiO_2 system. $H°_{f,298}$= enthalpy of formation from the elements at T_r=298.15 K, P_r = 1 bar; $S°_{298}$ = standard state entropy (T_r=298.15 K, P_r = 1 bar); C_P = isobaric heat capacity ($C_p = a + bT + cT^{-2} + dT^{-1/2} + eT^{-3} + fT^2 + gT^3 + hT^{-1}$). (1) this work; (2) Belmonte et al. [7].

Component	$H°_{f,298}$ (J/mol)	$S°_{298}$ (J/mol×K)	a	b × 10^3	c × 10^{-5}	d	e × 10^{-8}	f × 10^6	g × 10^9	h × 10^{-4}	Reference
CaO	−569918.0	56.0067	66.181	3.4509	14.209	−561.38	−3.6202	0.38087	−0.10247	0.26810	(1)
SiO_2	−911746.2	33.887	88.455	−3.00137	−48.527	−114.33	7.2829	0.71332	0.0059239	0.0	(2)

with reasonable accuracy. Because this system is of importance not only in Material Science but in the Earth Sciences as well, particular emphasis is devoted to the effects of pressure (P) as an intensive variable. Since few and, in some cases, controversial data exist on melting behavior and phase relations in the CaO-SiO_2 system, the main goals of this work are: (i) to assess a physically-consistent dataset of thermodynamic and thermophysical properties of liquid and solid phases in a broad range of P-T conditions; (ii) to define a theoretical framework (or, at least, some guidelines based on first principles) to properly combine thermodynamic with thermoelastic properties and account for first- and second-order (lambda) phase transitions; (iii) to compute relevant phase diagrams up to several tens of GigaPascals (GPa) and infer reliable stability relations both at subsolidus and melting conditions.

2. Ab initio-assisted thermodynamic modeling of pure solid and liquid phases

2.1. First-principles end-member properties

2.1.1. Liquid and glassy SiO_2

A computational investigation with ab-initio procedures of the structure-energy and vibrational properties of silica clusters in a dielectric continuum with dielectric constant ε=3.8 has shown that an aggregate of D_{6h} network units and $[SiO_4]^{4-}$ monomers, locally ordered in the short-medium range and in a mutual arrangement lacking of spatial continuity in the glassy state, reproduces satisfactorily both the experimentally observed low-T isobaric heat capacity and the deviation from the Debye T^3 law [12]. At the glass transition (T_g) the rotational and translational components generate a heat capacity gap only partly counterbalanced by the loss of coherent motion of all atoms in the ensemble [12]. The computation of the vibrational, translational and rotational components of the macroscopic partition function of the liquid, by assuming negligible anharmonicity, returns appropriate isochoric heat capacity values (C_V) at all T conditions within the homogeneity range of the substance. The discrete values may be then retrieved in terms of a modified Shomate's equation within a given T range (here arbitrarily expanded from 298.15 to 5000 K, or to 7000 K for solid and liquid CaO), i.e. $C_V = a + bT + cT^{-2} + dT^{-1/2} + eT^{-3} + fT^2 + gT^3 + hT^{-1}$. Thermoelastic properties (i.e. isothermal bulk modulus, K_T; volume thermal expansion coefficient, α_V; and molar volume at discrete temperatures, V) are then required to calculate the anharmonic contribution to the heat capacity (i.e. $TV\alpha_V^2K_T$), hence the isobaric heat capacity ($C_P = C_V + TV\alpha_V^2K_T$). Thermoelastic properties of the pure SiO_2 liquid were optimized on the basis of the low- to highpressure melting curve of the substance by Belmonte et al. [7], along the guidelines discussed in Ottonello et al. [13]. The substance was initially assumed to behave in a strictly harmonic way to reproduce the univariant curves experimentally observed at various P,T conditions. In the case of SiO_2, for instance, the liquidus was constrained to attain the melting point depicted by the experiments of Dalton and Presnall [14] at 5 GPa and to give melting temperatures roughly consistent with the experiments of

Shen and Lazor [15] at higher pressures. Initial guess values of the standard state molar volume (i.e. fictive liquid at T = 298.15 K and P = 1 bar), bulk modulus at the athermal limit (K_0) along with its baric and thermal derivatives (K'_0 and dK/dT, respectively), thermal expansion coefficient (represented as a polynomial expansion on T, $\alpha_V = \alpha_0 T + \alpha_1 + \alpha_2 T^{-1} + \alpha_3 T^{-2} + \alpha_4 T^{-3}$) were necessary to this purpose. The anharmonic contribution generated by the inverse procedure was retrieved in terms of a, c, f, and g coefficients of the Shomate's equation and then added to C_V in order to obtain C_P.

Calculations were iteratively refined to attain univariant loci consistent with the experimental observations. In this work we refined again the thermophysical properties of the liquid silica on the basis of a new ab initio-assisted assessment of the thermodynamic properties of αcristobalite, coupled with the effects of the α/β lambda transition (see Section 2.1.4.4 and Section 4.1). To achieve consistency with experiments over the entire P-range of interest (i.e. from 0 to 70 GPa) some thermophysical properties of liquid silica have been slightly changed with respect to our recent assessment [7]: the molar volume of the fictive liquid at standard state was lowered from 2.782 J/bar to 2.6 J/bar and the baric derivative of the bulk modulus was set to $K'_0 = 12.8$ (instead of 15.8). All the remaining thermodynamic and thermophysical parameters necessary to depict the properties of the liquid are the same as Belmonte et al. [7] (Tables 1, 2).

2.1.2. Liquid CaO

As observed by Bajgain et al. [16] through first principles molecular dynamics (FPMD) calculations carried out in the framework of Density Functional Theory (DFT) with plane-waves and pseudo-potentials, liquid CaO undergoes progressive structural changes with varying T and P. At low pressure the analysis of the partial Radial Distribution Function (RDF) suggests a mean coordination number around 5 for Ca-O first neighbours. This value progressively rises to RDF = 8 with the increasing pressure. According to the same Authors [16] the isochoric heat capacity of liquid CaO at 3000 K is $C_V = 44.90 \pm 1.83$ J/(mol×K). Based on the listed thermo-physical parameters at the same temperature, the anharmonic correction is $TV\alpha^2K = 21.77 \pm 2.75$ J/(mol×K), which gives an isobaric heat capacity $C_P = 66.67 \pm 4.58$ J/(mol×K) if added to the isochoric value. This value is consistent, within error, with the NIST-JANAF estimates [17], which assign to liquid CaO a constant heat capacity of 62.76 J/(mol×K). The melting temperature at 1-bar pressure is quite controversial. As emphasized by Eriksson et al. [18], older literature agrees in locating the melting point of CaO at $T_f = 2868 \pm 35$ K [19]. This value is accepted by a number of thermodynamic assessments [18,20–23], although other assessments [24,25] adopted a higher melting point at 1-bar pressure according to different experimental results (i.e. $T_f = 3200 \pm 50$ K [26] and $T_f = 3172$ K [27]). A recent experimental investigation by Manara et al. [28] confirms this higher melting temperature of lime (i.e. $T_f = 3222 \pm 25$ K at 1-bar pressure). The only molecular dynamics simulation made so far on CaO [29] adopts $T_f = 3200$ K and suggests a marked increase of the melting temperature with pressure (see later). The solid-liquid transition is poorly constrained also from the energy point of view. In the NIST-JANAF tabulations [17] the entropy of fusion of lime is

Table 2
Thermophysical properties of the pure liquid components in the CaO-SiO_2 system. $V°_{298}$ = standard state molar volume (T_r = 298.15 K, P_r = 1 bar); K_0 = bulk modulus at the athermal limit (i.e. T = 0 K; P = 0 GPa); $K'_0 = (dK/dP)_0$ = pressure derivative of the bulk modulus (assumed independent on T); $(dK/dT)_P$ = temperature derivative of the bulk modulus; α_V = volume thermal expansion coefficient ($\alpha_V = \alpha_0 T + \alpha_1 + \alpha_2 T^{-1}$).

Component	V°298 (cc/mol)	K_0 (GPa)	K'_0	$(dK/dT)_P$ (bar/K)	$\alpha_0 \times 10^7$ (K−2)	$\alpha_1 \times 10^7$ (K−1)	$\alpha_2 \times 10^3$
CaO	16.2	36	4.5	−45	0.0	1110	0.
SiO_2	26.0	5.0	12.8	0.0	−0.3611	843.1	0.

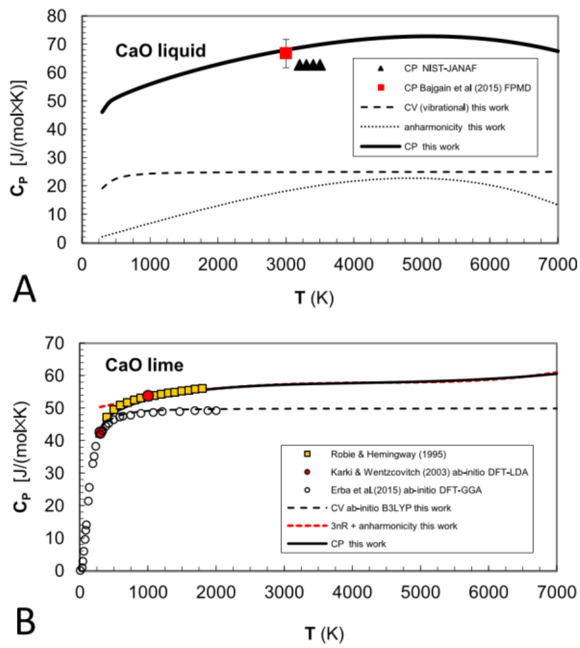

Fig. 1. Heat capacities of CaO liquid and solid phase (lime). (A) Bold, dashed and dotted lines represent C_P, vibrational C_V and anharmonicity (i.e. $TV\alpha_V^2K_T$) calculated for CaO liquid in this work, as compared with FPMD results [16] and NIST-JANAF tabulation [17]. (B) Ab-initio B3LYP isochoric heat capacity (C_V) and assessed isobaric heat capacity (C_P) of solid CaO (lime), as compared with calorimetric data [39] and other LDA [9] and GGA [38] calculations. The red dashed line, which represents the Dulong-Petit limit for C_P (i.e. $3nR + TV\alpha_V^2 K_T$), is drawn for illustrative purposes. (For interpretation of the references to color in this figure legend, the reader is referred to the web version of this article.)

assumed to be similar to that of periclase (MgO), i.e. ~6 cal/(mol×K). Also the heat capacity gap at T_f is controversial: quite small but positive when one adopts the heat capacity function of Berman et al. [30] for lime and the NIST-JANAF value for the liquid; negative, i.e. −0.672 J/(mol×K) at 3200 K, according to the tabulation of Barin [31]. The heat capacity gap at T_f is crucial in understanding the complex vibrational behavior of a substance at its melting point. In fact, the loss of coherent movement (i.e. acoustic motions) corresponds to a sudden increase of vibrational freedom (rotational and translational components) and also the anharmonic contributions may change substantially [2,12]. The vibrational heat capacity of the CaO crystalline phase has been calculated ab initio in this work by using a hybrid DFT functional (B3LYP) and a 6–31 G(d,p) basis set as implemented in the CRYSTAL code [32,33] (see Section 2.1.3 for details). The isobaric heat capacity of the liquid is then obtained by combining the vibrational heat capacity of the solid with the anharmonic contributions retrieved from the analysis of the CaO melting curve and with the 3 R contribution arising from the complete translational and rotational freedom of the atoms in the liquid. The resulting C_P of the liquid matches the FPMD prediction of Bajgain et al. [16] (Fig. 1a). The standard state values of thermodynamic properties for the liquid phase (i.e. enthalpy of formation from the elements at standard state, $H°_{f,298}$, and standard state entropy, $S°_{298}$; Table 1) were obtained by thermo-chemical cycle calculations assuming CaO to melt at 3222 K (see [1,13] for details). Based on our calculations the entropy of fusion is ~7 cal/mol [S_{fusion}= 29.207 J/(mol×K)], slightly larger than that of MgO (and in agreement with the fact that the former compound is more refractory). The bulk modulus of CaO liquid here adopted is consistent with the FPMD investigation of Bajgain et al. [16] (i.e. $K_0 = 24 \pm 2.5$ GPa at 3000 K), while its thermal derivative (i.e. dK/dT = −0.0045 GPa/K) has been assessed to flatten out the isobaric heat capacity at high T (Fig. 1a). The molar volume of the fictive liquid at room condition was obtained by adopting a constant thermal expansion coefficient (i.e. $\alpha_V = 1.11\times10^{-4}\ K^{-1}$), consistent with the observations of Bajgain et al. [16] at intermediate T (i.e. $\alpha_V = 1.167\times10^{-4}\ K^{-1}$ at 3000 K).

2.1.3. Solid CaO (lime)

As anticipated above, the vibrational properties of lime have been computed ab initio at B3LYP level of theory. The vibrational analysis at Γ point of the Brillouin zone gives the phonon frequencies of three optic modes: one doubly-degenerate transverse optic mode (i.e. $\nu_{4,5} = \nu_{TO} = 276.0$ cm^{-1};) and one longitudinal optic mode (i.e. $\nu_6 = \nu_{LO} = 552.4$ cm^{-1}). The calculated LO-TO splitting according to Born effective charges and dielectric tensor is 276.4 cm^{-1}, in excellent agreement with the experimental value obtained by neutron spectrometry (i.e. 263.6 ± 23.8 cm^{-1}) [34]. The acoustic frequencies at the Brillouin zone boundary (k_{max}) have been obtained from the elastic constant tensor analysis (i.e. $\nu_1 = 140.5$ cm^{-1}; $\nu_2 = 141.6$ cm^{-1} and $\nu_3 = 230.3$ cm^{-1}; see [35–37] for full details about the calculation method). Obviously the harmonic isochoric heat capacity strictly conforms to the Dulong-Petit limit at high temperature (i.e. 3nR, where n is the number of atoms in the unit formula of the substance and R is the gas constant) and practically overlap with the values obtained by a full phonon dispersion calculation [38] in the T range between 0 K and 2000 K (Fig. 1b). By adopting selected thermophysical parameters from the literature, the resulting isobaric heat capacity reproduces satisfactorily the experimental values of Robie and Hemingway [39] in the intermediate T range (Fig. 1b; Tables 3, 4). The Shomate's function for C_P conforms to the expected Dulong-Petit limit at high T (i.e. $3nR + TV\alpha_V^2K_T$): this is a compulsory requisite from a thermodynamic point of view, even though it is rarely fulfilled by the literature assessments.

To the best of our knowledge, the high-pressure melting curve of lime has never been determined by experiments. However, MD calculations predict a substantial increase of the melting temperatures with pressure [29]. We tuned the thermal derivatives of the bulk modulus of solid CaO in such a way to substantially reproduce the results of the MD simulation of Sun et al. [29] up to pressures of about 70 GPa, which is consistent with those realized in the Earth's lower mantle (Fig. 2 and Table 4).

2.1.4. SiO_2 polymorphs

The assessment of thermophysical properties for all SiO_2 polymorphs in this work, unless robust experimental data are available in the literature, is based on first-principles [12,40,41]. The adopted thermodynamic properties for most part of silica polymorphs are those of Berman [42]. This choice is dictated by the fact that the stability limits calculated for the low-density polymorphs of silica by Berman [42] adopting α-Quartz as reference phase for the enthalpy of formation from the elements of a large number of solids are still unmatched in their accuracy with respect to experiments. Furthermore, as we will see later on, the entropy of α and β polymorphs of cristobalite are in full agreement with first principles calculations. The effect of second-order (lamba) polymorphic transitions on the heat capacity of SiO_2 phases have been evaluated according to the procedure of Berman [42] by the following equation (applied for $T_{ref,\lambda} < T < T_\lambda$ at 1-bar pressure):

$$C_{P,\lambda} = T\cdot(X_{\lambda1} + X_{\lambda2}T) =^2 b\,T + f\,(T) + g\,(T_{\lambda\,\lambda} \quad ^2 \quad \lambda \quad)^3 \qquad (1)$$

where the parameters b_λ, f_λ and g_λ are those of the Shomate's equation for $C_{P,\lambda}$. All the parameters for lambda transitions of silica are given in Table 5.

Because the equation of state parameters of a substance are quite important in determining its extrinsic stability limits at planetary interior conditions (i.e. at very high P-T), the properties of the highest density crystalline polymorph (stishovite) assumes in our assessment a key role and will be outlined first.

2.1.4.1. Stishovite. In a previous work [41], we investigated ab initio the thermodynamic and thermophysical properties of stishovite, the

Table 3

Optimized thermodynamic properties of solid phases in the CaO-SiO_2 system. $H^0_{f,298}$= enthalpy of formation from the elements at T_r=298.15 K, P_r = 1 bar; S^0_{298} = standard state entropy (T_r=298.15 K, P_r = 1 bar); C_P = isobaric heat capacity ($C_p = a + bT + cT^{-2} + dT^{-1/2} + eT^{-3} + fT^2 + gT^3 + hT^{-1}$). The origin of the data and the optimization procedure adopted in this work are described in text.

Composition (Phase)	H0f,298 (J/mol)	S^0_{298} (J/mol×K)	a	b × 10^3	c × 10^{-5}	d	e × 10^{-8}	f × 10^6	g × 10^9	h × 10^{-4}
CaO (lime)	−645725.0	37.75	66.329	0.64172	19.122	−448.48	−3.7626	−0.43907	0.048879	−0.13326
SiO_2 (α-quartz)	−910700.0	41.460	80.01	0	−35.467	−240.3	4.9157	0	0	0
SiO_2 (β-quartz)	−908627.0	44.207	80.01	0	−35.467	−240.3	4.9157	0	0	0
SiO_2 (α-cristobalite)	−907753.0	43.394	83.51	0	−24.554	−374.7	2.8007	0	0	0
SiO_2 (β-cristobalite)	−906377.0	46.029	83.51	0	−24.554	−374.7	2.8007	0	0	0
SiO_2 (low-tridymite)	−907609.9	44.029	75.37	0	−59.581	0	9.5825	0	0	0
SiO_2 (mean-tridymite)	−907136.5	45.316	75.37	0	−59.581	0	9.5825	0	0	0
SiO_2 (high-tridymite)	−907045.0	45.524	75.37	0	−59.581	0	9.5825	0	0	0
SiO_2 (coesite)	−906662.0	40.668	97.552	−2.3932	−17.960	−634.24	3.8529	−0.65017	0.12384	−0.26112
SiO_2 (stishovite)	−874361.0	27.809	73.768	1.0205	−58.832	56.402	8.3752	0.65429	0	0
Ca_3SiO_5 (hatrurite)	−2938763.0	168.6	321.19	0	−9.948	−2450.2	0.9753	0	0	0
	−2308373.2	124.258	252.572	0	0	−2182.967	0	0	0	0

Ca_2SiO_4 (β-larnite)										
Ca_2SiO_4 (α' - bredigite)	−2303787.0	128.986	252.572	0	0	−2182.967	0	0	0	0
Ca_2SiO_4 (α - larnite)	−2291172.0	136.363	252.572	0	0	−2182.967	0	0	0	0
Ca_2SiO_4 (γ - Ca-olivine)	−2318090.3	115.582	252.572	0	0	−2182.967	0	0	0	0
Ca3Si207 (rankinite)	−3943000	210.874	339.91	0	−106.61	−985.1	13.7359	0	0	0
$CaSi0_3$ (wollastonite-I)	−1632094	81.81	149.07	0	−36.593	−690.3	4.8435	0	0	0
$CaSiO_3$ (pseudowollastonite)	−1628026	85.279	141.16	0	−58.576	−417.2	9.4074	0	0	0
$CaSiO_3$ (wollastonite-II)	−1626762	82.1	127.954	5.1129	−15.17495	0	0	0	0	0
$CaSiO_3$ (Ca-perovskite)	−1541000	74.0	114.66	9.8918	−19.527	−13.052	1.518	−02516	−0.15381	−0476251
$CaSi_2O_5$ (Ca-titanite)	−2482810	99.0	188.99	8.5971	−56.16397	0	0	0	0	0

rutile-type $P4_2/mnm$ tetragonal polymorph of silica, by hybrid DFT (B3LYP) calculations. It is well known that GGA-based hybrid density functionals slightly overestimate the molar volume at the athermal limit [43], so we adopted in this study the lowest experimental values, which range from 1.4000 to 1.4036 J/bar [44–49]. We extended here our previous quasi-harmonic mode-gamma analysis of the substance to a temperature of 5000 K (a value more consistent with the high-T regime that may be attained in planetary interiors):

$$\alpha K_T = \frac{ZR}{V}\sum_{i=4}^{3n} \gamma_i \frac{X_i^2 e^{X_i}}{\left(e^{X_i}-1\right)^2} \qquad (2)$$

where R is the gas constant, V is the molar volume, Z is the number of formula units in the unit cell, n is the number of atoms in the unit cell, X_i is the undimensionalized frequency of the i^th vibrational mode (i.e. $X_i = h\nu_i/kT$, where h and k represent Planck and Boltzmann constants, respectively, and ν_i is the radial frequency), and γ_i is the relative mode Grüneisen parameter of the i^th vibrational mode (i.e. $\gamma_i = \partial \ln \nu_i / \partial \ln V$) [37,50]. The analysis confirms that $\alpha K_T = f(T)$ has at high T a constant slope attaining 0.0059 GPa/K at T=5000 K. We kept our previous $\alpha_V = f(T)$ and reassessed the isobaric thermal derivative of the bulk modulus $(dK/dT)_P$ to achieve consistency over the entire T range of interest. The results of this assessment are resumed in Table 4. The bulk modulus at the athermal limit obtained in this way (K_0 = 270.1 GPa) is somewhat higher than the static value obtained by fitting the potential well (K_0 = 255.12 GPa) and intermediate between the values derived respectively from GGA and LDA calculations (see [40] and references therein). Because the anharmonicity at high T is slightly affected by the modified value for $(dK/dT)_P$, also the Shomate's parameters of the isobaric heat capacity were refitted by non-linear minimization procedures (Table 3). The compressional behavior of stishovite in a pressure range consistent with that attained in planetary interiors is shown in Fig. 3. Experimental observations in the low- to intermediate-P range [47,51,52] are superimposed for comparative purposes.

Fig. 4a shows the ab initio isochoric and isobaric heat capacities of stishovite at P =1 bar, compared with experimental observations for C_P in the low- to intermediate-T range [53–56]. Ab initio calculations are in good agreement with calorimetric data at intermediate temperature conditions (i.e. 300 K < T < 700 K), while some differences exist in the low-T range (i.e. at T < 300 K). Nevertheless, the latter are virtually irrelevant to the present assessment. The isobaric heat capacity C_P calculated in this work, besides being consistent with experimental data up to T ≅ 700 K, converge towards the Dulong-Petit limit dictated by anharmonicity at high T. The anharmonicity is definitely non negligible and attains ~14.7 J/(mol×K) at the maximum T of investigation. We

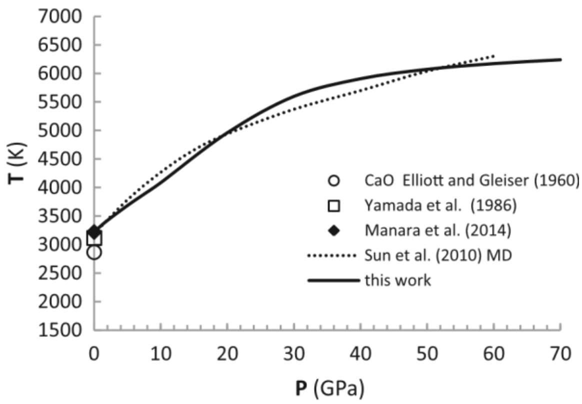

Table 4

Optimized thermophysical properties of solid phases in the CaO-SiO_2 system. V^0_{298}= standard state molar volume (T_r = 298.15 K, P_r = 1 bar). K_0 = bulk modulus at the athermal limit (i.e. T = 0 K; P = 0 GPa); $K'_0 = (dK/dP)_0$ = pressure derivative of the bulk modulus (assumed independent on T); $(dK/dT)_P$ and $(d^2K/dT^2)_P$ = first and second derivative of the bulk modulus with respect to temperature. $K_{0,T} = K_0 + T(dK/dT)_P + T^2(d^2K/dT^2)_P$ gives the temperature dependence of the bulk modulus. α_V = volume thermal expansion coefficient ($\alpha_V = \alpha_0 T + \alpha_1 + \alpha_2 T^{-1} + \alpha_3 T^{-2} + \alpha_4 T^{-3}$). The origin of the data and the optimization procedure adopted in this work are described in text.

Composition (phase)	$V0_{298}$ (cc/mol)	K_0 (GPa)	K'_0	$(dK/dT)_P$ (bar/K)	$(d^2K/dT^2)_P$ (bar/K^2)	$\alpha_0 \times 10^7$ (K−2)	$\alpha_1 \times 10^7$ (K−1)	$\alpha_2 \times 10^3$	α_3 (K)	α_4 (K^2)
CaO (lime)	16.76	130	4	−320.9	0.0251×2	0	501.25	−5.561	−0.4337	0
SiO_2 (α-quartz)	22.69	40.07	6	−53.678	0.0039	−0.6756	699.08	0	0	0
SiO_2 (β-quartz)	23.9	132.6	3.9	−1153.8	0.3218×2	−0.07	0	0	0	0
SiO_2 (α-cristobalite)	25.76	11.5	9	0	0	2.55	−2424.5	0	0	0
SiO_2 (β-cristobalite)	27.242	14.0	7.1	−20.	0	−0.173593	235.599	0	0	0
SiO_2 (low-tridymite)	27.170	30.8	4.1	0	0	−0.27655	313.204	0	0	0
SiO_2 (mean-tridymite)	27.170	30.8	4.1	0	0	−0.27655	313.204	0	0	0
SiO_2 (high-tridymite)	27.306	30.8	4.1	0	0	−0.27655	313.204	0	0	0
SiO_2 (coesite)	20.640	100.3	8.4	−249.584	0.0252×2	−0.004534	101.67	0	0	0
SiO_2 (stishovite)	14.000	270.1	6.59	−474.75	0.03514×2	0.05904	167.77	2.2872	−2.1518	237.0245
Ca_3SiO_5 (hatrurite)	72.740	97	4	−263.6	0.023×2	−0.0325	956.74	−20.0261	0	0
Ca_2SiO_4 (β-larnite)	51.600	125	4	−290	0.018×2	0.047	508.93	−5.412	0	0
Ca_2SiO_4 (α'- bredigite)	51.800	125	4	−290	0.018×2	0.047	508.93	−5.412	0	0
Ca_2SiO_4 (α - larnite)	53.600	125	4	−290	0.018×2	0.047	508.93	−5.412	0	0
Ca_2SiO_4 (γ - Ca-olivine)	57.500	122	4	−290	0.018×2	0.047	508.93	−5.412	0	0
Ca3Si207 (rankinite)	96.51	100.531	4	−100	0	−0.0028	363.56	−0.874	0	0
$CaSi0_3$	39.62	116.6	4	−330	0.027×2	0.04664	339.404	1.4588	−1.8634	0

(wollastonite-I)										
$CaSiO_3$ (pseudowollastonite)	40.08	113	4	−300	0.029×2	−0.013	466	−8.3137	0	0
$CaSiO_3$ (wollastonite-II)	37.94	93.9	5	0	0	0.01998	320	0	0	0
$CaSiO_3$ (Ca-perovskite)	27.45	239	4.8	−300 −376	0.01×2	0.01	300	0	0	0
$CaSi_2O_5$ (Ca-titanite)	48.192	178.2	4		0.039×2	0	350	0	0	0

Fig. 2. Melting curve of lime, as compared with the MD results [29]. Experimental data on melting point at P = 1 bar [19,27,28] are also shown for comparison.

adopted as standard state entropy of the substance the ab initio value determined by Ottonello et al. [41], i.e. $S°_{298}$ = 27.809 J/(mol×K), while $H°_{f,298}$ has been optimized in order to reproduce the high-pressure melting curve of the substance and, in particular, the invariant point at which stishovite coexists with liquid silica and coesite (see later). The calculated $H°_{f,298}$ is somewhat lower than current estimates (i.e. −874.4 kJ/mol against −861.3 kJ/mol according to Robie and Hemingway [39]) but consistent with the assessment of Mao et al. [57].

2.1.4.2. Coesite. With the decrease of P at subsolidus conditions, stishovite transforms reversibly into the less dense phase coesite. The adopted space group of monoclinic coesite is C2/c [58,59], though the space group $P2_1/c$ has also been proposed [60]. Ab-initio LDA calculations give K_0 = 94.3 GPa and K'_0 = 4.8 for the bulk modulus of coesite and its pressure derivative, respectively [40]. These compressibility values are only approximately consistent with the experimental observations of Levien and Prewitt [61] and the assessment of Mao et al. [57]. A slightly higher bulk modulus and baric derivative (i.e. K_0 = 100.3 GPa, K'_0 = 8.4) have been preferred in this work, along with a marked T-depencence of the compressibility (i.e. dK/dT = −249.584 bar/K; d^2K/dT^2 = 0.0504 bar/K^2) (Table 4). The standard state molar volume and the thermal expansion here adopted are based on the experiments of Bourova et al. [62] and in reasonable agreement with other experimental data [63,64] (Fig. 5). The isobaric heat capacity (Fig. 4b) is essentially based on the experiments of Hemingway et al. [65], refitted in the form of a Shomate's equation consistent with the Dulong-Petit limit at high T.

Table 5

Thermodynamic parameters describing polymorphic lambda transitions in SiO_2 and Ca_2SiO_4 according to Eq. (1). The enthalpy of transition, modeled as first order ($\Delta H_{1st\ order}$) and the Clapeyron slope of the phase boundaries (dT/dP) are also indicated. Some literature values (in parentheses) are shown for comparison.

low-T polymorph	Tλ	Tref	$X\lambda_1$	$X\lambda_2$	bλ	fλ	gλ	dT/dP	ΔH1st order	References
	(K)	(K)						(K/bar)	(J/mol)	
SiO_2 (α-quartz)	848	373	−0.09187	0.00024607	0.008440	−4.52129E−05	6.05504E−08	0.02565	499	this work
								(0.0237)		Berman [42]
									(499)	Berman and Brown [70]
SiO_2 (α-cristobalite)	550	298.15	−0.1	0.0004465	0.010000	−8.000000E−5	1.60000E−07	0.1217	304	this work
SiO_2 (low-trydimite)	388	304	−0.83	0.0027311	0.705600	−4.586000E−3	7.452900E−6	0.0	–	this work
SiO_2 (mean-trydimite)	440	388	−0.52	0.0014	0.270400	−1.456000E−3	1.96000E−06	0.0655	–	this work
α'-Ca_2SiO_4	1710	970	−0.22815	0.00023196	0.052052	−1.058400E−4	5.38054E−08	0.023	12615	this work

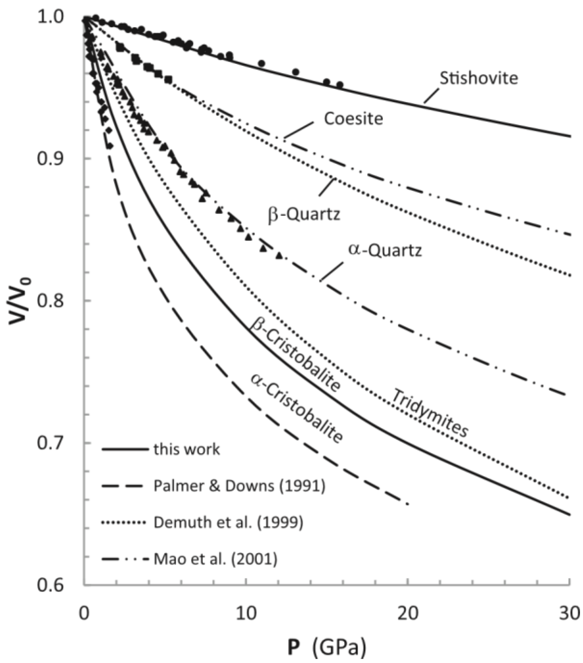

Fig. 3. Compressional behavior of silica polymorphs: assessments (this work, Demuth et al. [40], Mao et al. [57]) and experiments. Experimental data for stishovite: Ross et al. [47], Olinger [51], Liu et al. [52]; coesite: Levien and Prewitt [61]; α-quartz: Vaidya [76], Olinger and Halleck [77], D'Amour et al. [78], Levien et al. [79], Cartz and Jorgensen [80], Jorgensen [81]; α-Cristobalite: Downs and Palmer [84].

Based on the above selected thermophysical parameters and differently from stishovite, the anharmonicity contribution to the isochoric heat capacity is almost negligible. The assessed values of $S°_{298}$ and $H°_{f,298}$ are nearly similar to those of Mao et al. [57].

2.1.4.3. Quartz. Coesite transforms reversibly to β-quartz by decreasing the pressure at T > 1550 K and to α-quartz at lower T. The assessment of the thermophysical properties of the α-β polymorphs of quartz is complicated by the existence of a lambda transition coupled to a slight first-order contribution. The λ-transition of quartz has been treated in many ways with somewhat contradictory results in terms of 2nd order contributions to the bulk thermodynamic properties of the phase [42,66–70]. We adopted here the procedure of Berman [42]: a common background heat capacity (or "lattice" contribution [42]) with superimposed λ-contributions. According to the experiments of Ackermann and Sorrell [71] and Bourova and Richet [72] the standard state molar volume of β-quartz was set to 23.9 cc/mol and assumed to be affected by a small negative thermal expansion represented by a single numerical coefficient (i.e. $\alpha_V = -0.07\times T$; Table 4). The simple 1st-order treatment of the α-quartz to βquartz transition gives a constant Clapeyron slope dT/dP = 0.02565 K/ bar (Table 5). The λ-contribution to entropy at the critical temperature

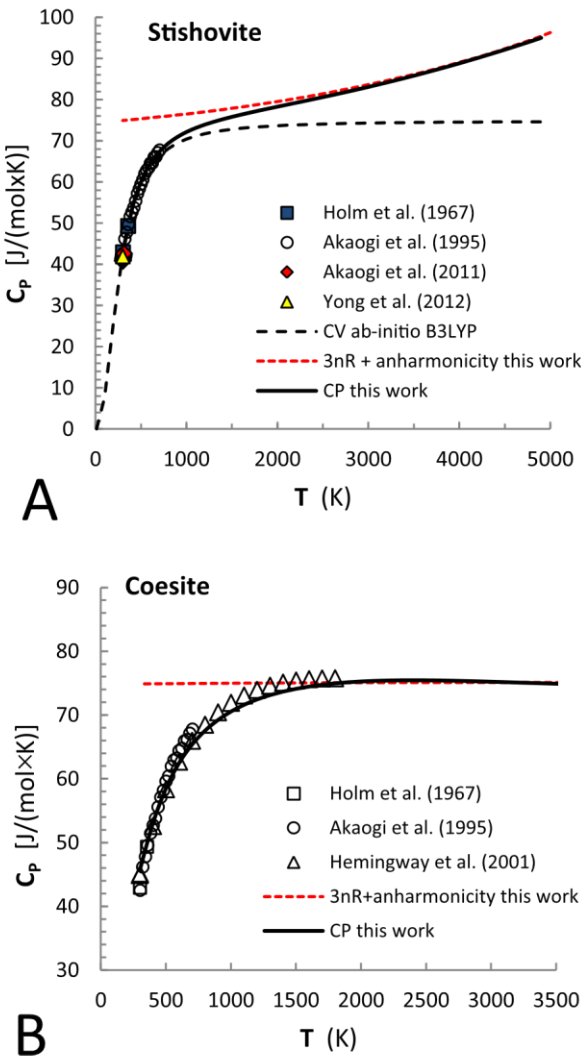

Fig. 4. Calculated heat capacities of stishovite (A) and coesite (B), compared with calorimetric data in the low-T [53–56] and intermediate-T [56,65] range. Solid curves are the continuous functions generated by the Shomate's heat capacity polynomial expansion valid up to the high thermal regimes of interest in this study. Red dashed lines, which represent the Dulong-Petit limit for C_P of stishovite and coesite (i.e. $3nR + TV\alpha_V^2K_T$), are drawn for illustrative purposes. (For interpretation of the references to color in this figure legend, the reader is referred to the web version of this article.)

($T_C \cong T_\lambda = 848$ K) is $S_{\lambda,C} = 2.158$ J/(mol×K). The volume change at the lamba transition point is $V_{\lambda,C} = 0.554$ cc/mol, which, if subtracted to the 1st-order volume of β-quartz at T_λ and scaled to ambient conditions according to thermal expansion of the α-polymorph, returns $V°_{298} = 22.95$ cc/mol for α-quartz (see Fig. 5). This value is still somewhat higher than the observed value of Taylor [73] (i.e. $V_0 = 22.69$ cc/mol),

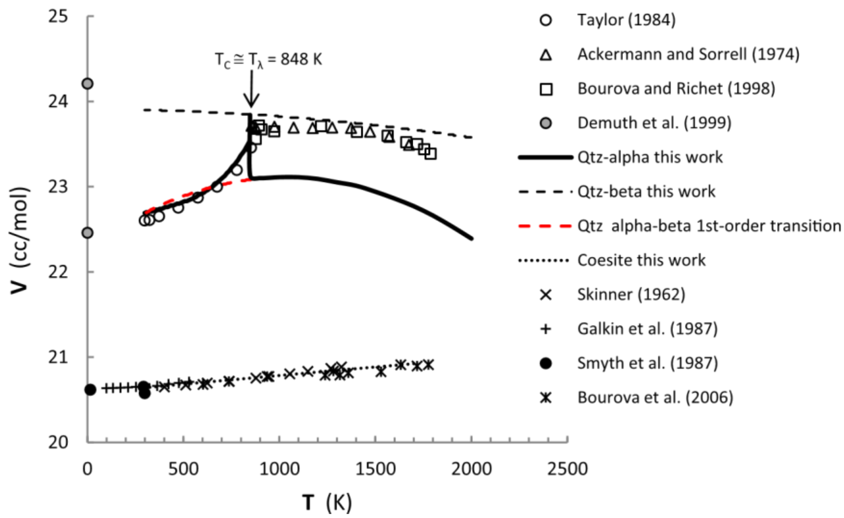

Fig. 5. Molar volumes of quartz and coesite as modeled in this work, compared to experimental observations [58,62–64,71–73] and first principles computations [40]. The red dashed line depicts the fictive volume of the α-quartz polymorph in the absence of the effects of the displacive phase transition to β-quartz at P = 1 bar. $T_C \cong T_\lambda$ = 848 K is the critical temperature for the α-β quartz phase transition. (For interpretation of the references to color in this figure legend, the reader is referred to the web version of this article.)

which is here preferred. Nonetheless, as shown in Fig. 5, the volume thermal expansion of α-quartz below the phase transition is sufficiently consistent with experiments.

The potential well of the $P6_222$ structure of β-quartz as determined by DFT-LDA computations [40] indicates a marked stiffness of the substance at the athermal limit (i.e. K_0 = 132.6 GPa), while an unique experimental observation at relatively high temperature gives K_T = 56.4 GPa at T = 873 K [74]. A strong T-dependence of the bulk modulus can thus be inferred for β-quartz, which was interpreted by Demuth et al. [40] as due to the activation of low-frequency Rigid Unit Modes (RUMs). For the $P3_221$ α−polymorph the same Authors [40] calculated a static bulk modulus of 35.4 GPa by LDA [40], while Hamann [75] obtained K_0 = 45.0 GPa at the same level of theory. We adopted here the assessment of Mao et al. [57], which assign K_0 = 40.07 GPa and K'_0 = 6.0 on the basis of several sets of internallyconsistent experiments [76–81] (Fig. 3 and Table 4). As concerning the thermal dependence of the bulk modulus, we adopted the assessed value of Mao et al. [57] for α-quartz, while we optimized the $(dK/dT)_P$ value for β-quartz on the Clapeyron slope of the experimental phase boundary between the two polymorphs according to Cohen and Klement [82] and Mirwald and Massonne [83] (Table 4). The ensuing anharmonicity is definitely non negligible and attains ~2.3 J/(mol×K) at T = 3000 K. The isobaric heat capacity is below the Dulong-Petit asymptotic limit at all T of interest (see Fig. 1-SM in Supplementary material).

2.1.4.4. Cristobalite. We adopt for the α-polymorph (space group $P4_12_12$) the thermoelastic parameters of Downs and Palmer [84] (i.e. V_0 = 25.76 cc/mol; K_0 = 11.5 GPa; K'_0 = 9.0). The experimental bulk modulus is in agreement with DFT-LDA calculations of Teter et al. [85] and Demuth et al. [40] (i.e. 11.9 and 12.8 GPa, respectively), though the baric derivative is much higher than the computed ones (3.0 and 6.3, respectively). K_0 and K'_0 of the β-polymorph are those obtained by Demuth et al. [40] on the $P2_13$ cubic phase (i.e. K_0 = 14.0 GPa; K'_0 = 7.1). The adopted standard state volume (V_0 = 27.242 cc/mol) and thermal expansion of β-cristobalite are consistent with the observations of Swainson and Dove [86] and Bourova and Richet [72] (Fig. 6 and Table 4).

To reproduce the experimental Clapeyron slope of the α/β transition [87,88] we must assume that the α-polymorph has a complex thermal expansion (α_V negative from room temperature to T ≅ 950 K

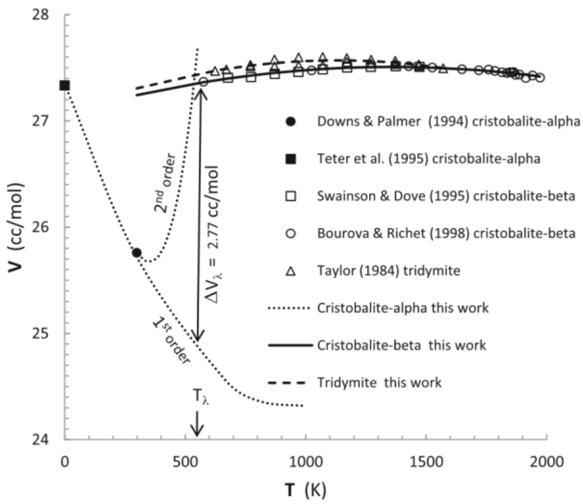

Fig. 6. Molar volumes of cristobalite and tridymite as modeled in this work, compared to experimental observations [72,73,84,86] and first principles calculations [85]. The effect of the lamba displacive phase transition on the molar volume of the α polymorph at T_λ (i.e. $\Delta V_\lambda = 2.77$ cc/mol) is also sketched.

and positive at higher T; Fig. 6). This complex behavior is consistent with our calculated displacive contributions to volume at T_λ (i.e. $\Delta V_\lambda = 2.770$ cc/mol based on the Clapeyron slope; cf. Fig. 6 and Table 5; see also Section 4.1). The λ-transition from the α to β polymorph induces a substantial increase in the heat capacity up to a critical limit that, according to Mosesman and Pitzer [89], would attain ~23 J/(mol×K) at 550 K (see Fig. 2-SM in Supplementary material). Based on our modeled transition (see Table 5 and Fig. 2-SM), the delta in the bulk entropy of the two polymorphs is 2.276 J/(mol×K) at this temperature and the β-polymorph has a standard state entropy $S^\circ_{298} = 46.029$ J/ (mol×K), which is consistent with the assessed value of Berman [42]. The "lattice" heat capacity function of Berman [42] is still below the Dulong-Petit asymptotic limit in the T-range of extrinsic stability of the substance (Fig. 2-SM).

2.1.4.5. Tridymite. The low-density polymorphs of silica known as "tridymites" occur in a variety of space groups, hence numerous phase transitions have been proposed [89–92]. The high-T polymorph is closely related to the β-cristobalite structure [93]. The ideal $C222_1$ orthorhombic structure of β-tridymite has been investigated by DFTLDA calculations [40], which give $K_0 = 30.8$ GPa and $K'_0 = 4.1$. The experimental data of Taylor [73] on thermal expansion of tridymite may be reproduced with a simple two-parameters polynomial function (i.e. $\alpha_V = \alpha_0 T + \alpha_1$, with $\alpha_0 = -0.276E{-}07$ and $\alpha_1 = 313.2E{-}07$) and a standard state molar volume $V_0 = 27.306$ cc/mol (cf. Fig. 6 and Table 4). Following Berman [42] one

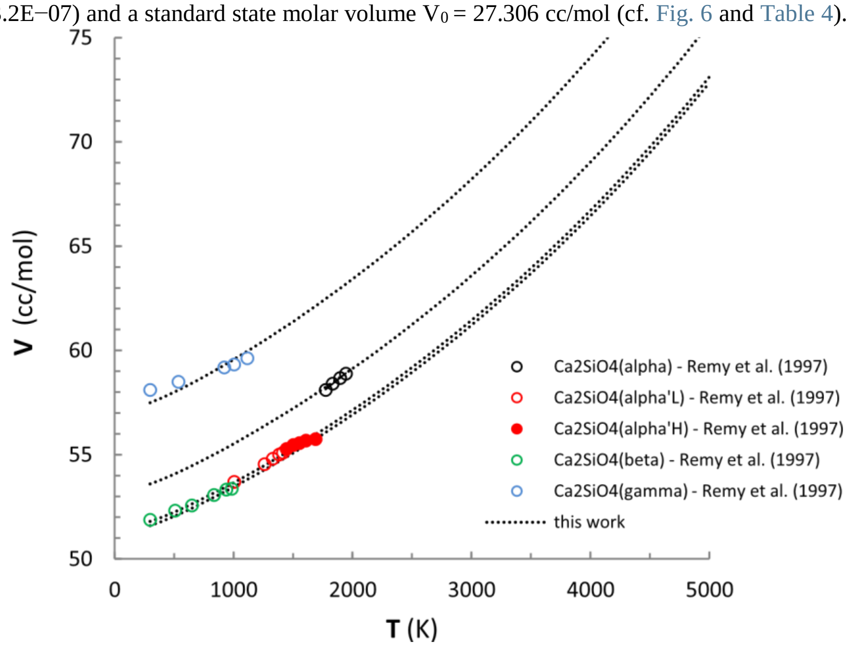

Fig. 7. Volume thermal expansion of Ca_2SiO_4 solid polymorphs as modeled in this work (dotted lines), compared to the discrete experimental values of Remy et al. [97].

could assume that only two phase transitions occur in tridymites, namely those for which "acceptable consensus" exists: a low-to-mean transition occurring at $T_\lambda = 388$ K and a mean-to-high transition at $T_\lambda = 440$ K [91,92]. We assumed for simplicity that the thermophysical parameters of the "low" and "mean" polymorphs are identical to those of the "high" polymorph here identified with the ideal $C222_1$ orthorhombic structure. The common "lattice" heat capacity function of tridymite [42] is shown in Fig. 3-SM of Supplementary material with the two lamba phase transitions superimposed (see also Table 5). The 2nd order contributions of the two λ-transitions at T_λ are the following: ΔH_λ = 543 J/mol, ΔS_λ = 1.479 J/(mol×K), ΔV_λ = 0.0 J/bar for the low/mean transition at T_λ = 388 K; ΔH_λ = 88 J/mol, ΔS_λ = 0.208 J/(mol×K), ΔV_λ = 0.0136 J/bar for the mean/high transition at T_λ = 440 K.

2.2. Intermediate crystalline compounds

Besides lime and the polymorphs of silica, other thirteen compounds are known to nucleate in the system: hatrurite (Ca_3SiO_5), five polymorphs of the Ca_2SiO_4 orthosilicate [α'_H, α'_L, α (bredigite), β (larnite), γ (Ca-olivine)], rankinite ($Ca_3Si_2O_7$), Ca-titanite ($CaSi_2O_5$) and five polymorphs of the $CaSiO_3$ metasilicate (wollastonite, pseudowollastonite, walstromite, wollastonite-II, Ca-perovskite). The extrinsic stability relations of solid phases at subsolidus in the wide P,T regime of interest in geophysical investigations are quite complex and affect melting relations as well.

2.2.1. Ca_2SiO_4

Ca_2SiO_4 is an important constituent of Portland cement [94–96] and, as such, it has been extensively investigated. The extrinsic stability relations at room pressure are still matter of debate. The stable form at low T and ambient P is orthorombic (γ-Ca_2SiO_4, Ca-olivine) but it is readily replaced by a monoclinic form (β-Ca_2SiO_4, larnite) with increasing pressure (see Section 4.4). The α'_H and α'_L orthorombic polymorphs are stable at intermediate T (from ~1000 K to ~1700 K) and finally transform into the α polymorph (α-larnite), whose crystal symmetry is still uncertain (trigonal or exagonal; see Remy et al. [97] and references therein). α-Ca_2SiO_4 melts at 2403 K at room pressure. Complex extrinsic stability relations have been proposed in [98], which we would refer the interested reader to. As common lattice heat capacity of β, α', α, γ polymorphs we adopted the simple twoparameters C_P=f(T) function of Berman and Brown [99] for the α' polymorph (see Table 3). This function conforms rather well even to extreme temperature conditions (see Figs. 4a-SM, 4b-SM, 5-SM and 6SM in Supplementary materials).

The β-α' transition was modeled by Berman and Brown [69] as pure first-order phase transition with a transition enthalpy $H_{trans,\beta\text{-}\alpha'}$ = 1748 J/mol at $T_{trans,\beta\text{-}\alpha'}$ = 970 K. The α'-α transition has a superimposed λ- and 1st-order character, with a sensible 1st-order contribution equal to $H_{trans,\alpha'\text{–}\alpha}$ ~12.6 kJ/mol at $T_{trans,\alpha'\text{–}\alpha}$ = 1710 K (Table 5 and Fig. 4b-SM in Supplementary materials).

We disregarded the α'_H-α'_L transition for the difficulty in retrieving satisfactory thermophysical parameters for these very similar polymorphs and we treated α' as a single phase. The adopted $H°_{f,298}$ and $S°_{298}$ for all the Ca_2SiO_4 polymorphs were initially chosen according to Haas et al. [100]. In a subsequent optimization the parameters were readjusted to conform to the observed extrinsic stability limits. The assessment of the thermophysical properties was essentially based on the observations of Remy et al. [97], with some limited modifications to attain the Dulong-Petit asymptotic limit at high T. Since the existing experimental data on thermal expansion of the Ca_2SiO_4 solid polymorphs [97 and references therein; 101–103] are quite scattered (see Fig. 7-SM in Supplementary materials), the choice of a "generalized" thermal expansion (i.e. common to all the polymorphs) was almost compulsory. After this quite crude selection, we compared the expanded volumes calculated with a common α_V polynomial function to the discrete experimental values of Remy et al. [97], then we optimized consistently a standard state volume for each of the polymorphs (see Fig. 7 and Table 4).

2.2.2. $CaSiO_3$

As for Ca_2SiO_4, also $CaSiO_3$ exhibits extensive polymorphism which has been the object of different experimental investigations. The polymorph stable at room condition is wollastonite (triclinic, space group $P\bar{1}$). According to Richet et al. [104] there is a reversible transition from low-wollastonite to high-wollastonite at T = 995 ± 10 K, which is clearly detectable in the mean heat capacity values (see Fig. 1 in [104] and references therein). The transition "can be considered calorimetrically as first order" (Richet et al. [104]) with a very small enthalpy of transition (i.e. ~200 J/mol). Wollastonite (Wo) undergoes a solid-state phase transition to monoclinic pseudowollastonite (PWo): according to the experimental observations of Kushiro [105] the phase transition at ambient pressure is predicted to occur at T = 1398 ± 10 K. According to Osborn [106] pseudowollastonite melts congruently at 1817 K (or 1821 K by correction on the 1968 International Temperature Scale, [104]). Barin [31] lists an enthalpy of fusion of 56.066 kJ/mol at T = 1816 K for $CaSiO_3$. A similar value was obtained by Adamkovikova et al. [107] by solution and dropcalorimetry experiments (57.3 ± 2.8 kJ/mol). At high pressure (i.e. roughly above 2.5 GPa), PWo transforms into another triclinic polymorph: wollastonite-II (Essene [108]; Wo-II). Wo-II is structurally quite similar to another high-pressure polymorph of $CaSiO_3$ (walstromite), where "the axial ring Si_3O_9 is isomorphously replaced by the same ring with the inverse axiality" [109]. Above ~10 GPa the stable phase of $CaSiO_3$ is orthorhombic (space group Pnma), and generally indicated as "Ca-Perovskite" (Ca-Pvsk). For Wo and PWo we adopted the heat capacity coefficients of Berman [42], which are based essentially on the calorimetric measurements of Krupka et al. [110,111], White [112], Wagner [113], Elsner von Gronow and Schwiete [114] and disregard the low- to high-wollastonite phase transition detected by Richet et al. [104]. We note however that below ~1000 K the low-wollastonite data of Richet et al. [104] are consistent with the heat capacity function selected in this work and a good consistency is observed also for PWo up to ~2000 K (see Fig. 8-SM in

Supplementary materials). The assessment of Berman [42] was initially adopted also for the enthalpy of formation from the elements at standard state and the standard state entropy of Wo and PWo. In our assessment $H°_{f,298}$ of both polymorphs was lowered by ~0.6 kJ/ mol. We did not make any distinction between wollastonite-II and $CaSiO_3$-walstromite due to their structural similarity. The heat capacity of Wo-II is shown in Fig. 9-SM of Supplementary materials along with that of the Ca-perovskite phase. The heat capacity equation provided by Swamy and Dubrovinsky [115] was initially adopted for Wo-II and Capvsk, but, when coupled with the thermophysical parameters selected or refined in this study, a slight (Wo-II) or marked (Ca-Pvsk) discrepancy with respect to the asymptotic Dulong-Petit limit at high T was evident and a partial refitting was deemed as necessary (Table 4 and Fig. 8-SM of Supplementary material). For Wo-II we adopted the standard state molar volume of Chatterjee et al. [116] and the thermal expansion of Swamy and Dubrovinsky [115]. The bulk modulus and its thermal derivatives were refined in this study on the basis of the Wo/ Wo-II subsolidus univariant curve (see Section 4.5 for details). As to Ca-pvsk, we adopted the standard state molar volume of Wang et al. [117], while thermal expansion and isothermal compressibility were fully refined according to the vibrational constraint on C_P given by the Dulong-Petit limit at high T.

2.2.3. Ca_3SiO_5

Thermodynamic properties of Ca_3SiO_5 (hatrurite) are quite controversial in the literature [18,20,31,39,69,99,118–120]. In this work we adopted the $S°_{298}$ value of Barin [31], the heat capacity of Berman and Brown [69,70] and the standard state molar volume of Robie and Hemingway [39]. With respect to our previous optimization [13], we slightly modified the thermal expansion of Skinner [121] to render the anharmonicity of the substance consistent with the $C_P = f(T)$ function at high temperature (Table 4). The attainment of the expected DulongPetit asymptotic limit was thus satisfied (Fig. 10-SM in Supplementary materials). Furthermore, we decreased the $H°_{f,298}$ value to −2938.763 kJ/mol with respect to calorimetric results [39,118] (Table 3) in order to get meaningful liquidus and subsolidus phase relations both at ambient and high-pressure conditions (see Sections 4.6 and 4.7).

2.2.4. $Ca_3Si_2O_7$

As for Ca_3SiO_5, thermodynamic properties of $Ca_3Si_2O_7$ (rankinite) are affected by a large uncertainty [18,118,119,122,123]. We adopted for $H°_{f,298}$ a value nearly similar to that assessed by Eriksson et al. [18], while $S°_{298}$ is that of Barin [31]. As for most part of the other intermediate compounds, the Shomate's coefficients for C_P are those of Berman and Brown [69,70]. $V°_{298}$, K_0 and K'_0 values are those assessed by Holland and Powell [124], while thermal expansion was initially set according to the estimates of Skinner [121] and then refined to conform the anharmonicity of the substance to the asymptotic Dulong–Petit limit at high T (see Fig. 11-SM in Supplementary materials).

2.2.5. $CaSi_2O_5$

Ca-titanite ($CaSi_2O_5$) forms by breakdown of Wo-II above ~8– 9 GPa [125]. This phase coexists at subsolidus equilibrium conditions with β-Ca_2SiO_4 (larnite) in a limited pressure range. Above 11–13 GPa the $CaSi_2O_5$ + β-Ca_2SiO_4 equilibrium assemblage recombines into the high-density polymorph of $CaSiO_3$ (Ca-Pvsk). As far as we know, there are no firm estimates of the isobaric heat capacity of Ca-titanite, besides the quasi-harmonic lattice dynamics simulation of Swamy and Dubrovinsky [115] which is here adopted (Table 3). According to Angel and coworkers [126–128], $V°_{298}$ = 48.192 cc/mol, K_0 = 178.2 GPa and K'_0 = 4.0. A more recent ab initio investigation [129] defines a lower (static) value for the bulk modulus (i.e. K_0 = 152 GPa), while confirming the baric derivative. In order to have a $TV\alpha_V^2K_T$ anharmonic term consistent with the adopted isobaric heat capacity (cf. Fig. 12-SM in Supplementary material) one must assume a marked value for the thermal derivative of the bulk modulus (Table 4). In that case, the expected K_0 at the athermal limit would be much higher than the computed value by Yu et al. [129]. Therefore we assumed K_0 = 178.2 GPa according to Angel et al. [128]. The $H°_{f,298}$ adopted in this work is the calorimetric value of Schoenitz et al. [130] (Table 3), which is consistent with that of Akaogi et al. [131] within experimental uncertainty. The remaining parameters were refined in this study to reproduce the univariant phase equilibrium boundaries $CaSi_2O_5$ + βCa_2SiO_4 = $CaSiO_3$ (Wo-II) and $CaSi_2O_5$ + β-Ca_2SiO_4 = $CaSiO_3$ (Capvsk) at subsolidus conditions, according to the experimental observations of Kanzaki et al. [132] and Gasparik et al. [125] (see also Section 4.5).

3. The CaO-SiO_2 liquid

Interactions at the liquid state were modeled with the Hybrid Polymeric Approach (HPA) [133,134]. The model is basically a slight modification of the Toop-Samis model [135,136] and its application has been extensively discussed elsewhere [7,13]. We simply recall that the Gibbs free energy of mixing (G_{mix}) of a multi-component liquid can be obtained as a sum of discrete contributions arising from different kinds of interaction among chemical species in the structure of a polymeric substance. The different energy terms are represented by a dominant chemical interaction among polymeric units ($G_{chemical}$) and subordinated interactions in the cation and anion matrices ($G_{cat.mix}$ and G_{strain}, respectively):

$$Gmixing = Gchemical + Gcat.mix + Gstrain \qquad (3)$$

The chemical interaction is related to a polymerization constant (K_P) which is in turn intimately linked to the donor pressure of the system depending on the contrast in the Lux-Flood acid-base characters of the oxygen donors (or "Network Modifiers", NM) and oxygen acceptors (or "Network Formers", NF)

$$G_{chemical} = \frac{(O^-)}{2} RT \ln K_P \qquad (4)$$

Table 6
Parameters of the Hybrid Polymeric Approach for the $CaO\text{-}SiO_2$ system. A and B represent enthalpic and entropic contributions, respectively, to the polymerization constant K_P (see Eq. (6)). $\eta_{k,S}$ and $\eta_{k,V}$ are strain parameters according to Eqs. (9) and (10) (see text for details).

A	−14416
B	0
$\eta_{1,S}$	−2.5
$\eta_{5,S}$	8
$\eta_{0,V}$	0.0573–0.3473/P [P (GPa) ≤ 1]
$\eta_{5,V}$	1.013–0.013×P [P (GPa) ≤ 1]

$$K_P = \frac{(O^{2-})\cdot(O^0)}{(O^-)} \qquad (5)$$

where (O^{2-}), ($O°$) and (O^-) are the activities of free oxygens, bridging oxygens and singly-bonded (non-bridging) oxygens, respectively, and (O^-)/2 accounts for the number of contacts between the functionals of the polymeric units. In a NM-NF system of highly contrasting acid-base character such as $CaO\text{-}SiO_2$ the chemical interaction is expected to be mainly enthalpic in nature. Because the polymerization constant K_P in the HPA model is expanded in the form:

$$\ln K_P = A/T + B \qquad (6)$$

the A and B coefficients acquire a precise thermodynamic significance, with R×A and -R×B representing respectively the enthalpic and entropic contributions to the chemical interaction energy between NM and NF per unit mole of contacts. In our case, from the topological analysis of the binary phase diagram it turns out that B is virtually zero, so the chemical interaction is completely enthalpic (Table 6). The heat of mixing arising from the A model parameter may be compared with the heat of mixing of discrete solid compounds in the system by applying:

$$H_{mixing,Tf} = \frac{H_{solid,Tf} + H_{fusion} - \sum n_i \mu_i^{0,liquid,Tf}}{\sum_i n_i} \qquad (7)$$

where H_{fusion} is the heat of fusion, $\mu_i°$ and n_i are the standard state chemical potentials and the number of moles per formula unit of the i^{th} oxide in the liquid and the corresponding solid, respectively. We may thus see that the heat of mixing of the $CaO\text{-}SiO_2$ binary liquid is quite consistent with the heats of fusion of the ortho- and meta-silicate phases (i.e. α-Ca_2SiO_4 bredigite and $CaSiO_3$ pseudo-wollastonite [31,107]) (see Fig. 8). The strain contribution to the bulk Gibbs free energy of mixing is

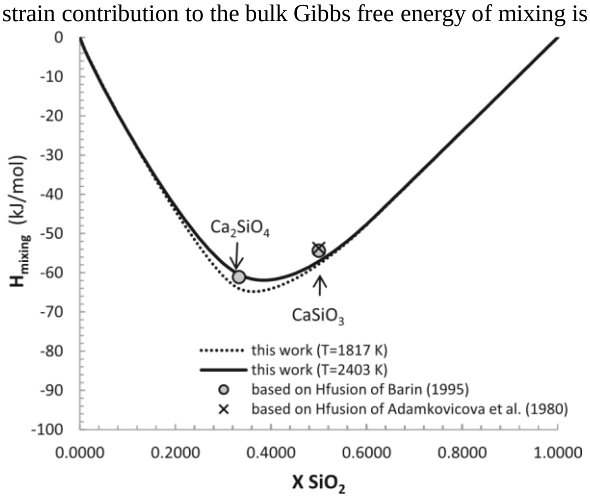

Fig. 8. HPA heat of mixing along the CaO-SiO_2 join calculated at T = 2403 K and T = 1817 K (solid and dotted curves, respectively). The values expected from the experimental latent heats of fusion of the two pure compounds at T_f [31,107] are superimposed for comparison.

quite limited (Table 6). Since G_{strain} is related to the medium-range disorder of polymeric units in the anion matrix, it can be obtained as follows:

$$G_{strain} = \frac{(O^-)}{2}\eta \qquad (8)$$

where η is a strain parameter which is conveniently expanded as a function of the molar fraction of Network Formers in the system (X_{NF}) and intensive variables P,T, i.e.

$$\eta = \sum_{k=0}^{n} \eta_k \cdot (2X_{NF} - 1)^k \qquad (9)$$

$$\eta_k = \eta_{k,H} - T \cdot \eta_{k,S} + P \cdot \eta_{k,V} \qquad (10)$$

This limited amount of energy operates only over the acidic part of the system (i.e. $X_{NF} = X_{SiO_2} \geq 0.5$, where polymeric units are present) and is thus set to zero for the remaining part of the system.

The volume terms described by $\eta_{k,V}$ in Eq. (10) depict a Pdependent excess volume (V_{exc}), constrained by experimental observations at discrete P conditions. The excess volume is slightly negative at low P and progressively vanishes with increasing pressure (V_{exc} becomes virtually zero at P > 1 GPa; see Table 6). At variance with the enthalpic and entropic contributions, the volume terms operate over the entire compositional space because intimately connected with the short-range properties of the pure components, affected in a complex way by pressure. Finally, as anticipated long ago [133], though the eigenvalues of the Toop-Samis model [135,136] nominally cover the entire compositional range from pure NM to pure NF, they are unphysical below a certain NF amount because they would imply decomposition of monomers, which is energetically unlikely [4,137]. The procedure adopted by the HPA model to solve this inconsistency, along with its implications, is briefly discussed in Supplementary material.

A simplified FORTRAN routine to build up phase diagram topology, based on a more complex procedure adopted for high-rank simplexes [7,13,36], is available upon request to G.O. (DISTAV, University of Genova, Corso Europa 26, 16132 Genova, Italy; e-mail: giotto@ dipteris.unige.it).

4. Results and discussion

4.1. The SiO_2 phase diagram at low pressure

Although the thermochemical parameters (i.e. C_P, $H°_f$, S_0) adopted for the low-density polymorphs of silica (tridymites, α/β cristobalite, α/ β quartz) are those of Berman [42] their thermophysical properties were completely revised, due to physical unsoundness, by taking into account all available experimental evidences (see Sections 2.1.4.3– 2.1.4.5). Notwithstanding this revision, the new extrinsic stability limits between the various polymorphs keep a reasonable consistency (Figs. 9a, b and 10). As we may see for instance in Fig. 9a and b the Clapeyron slopes between tridymite and cristobalite polymorphs are well reproduced within the limits of reversal experiments

[87,88,91,92]. It should be stressed that, in the case of phase transition with a wide T_{ref}-T_λ gap and a marked Clapeyron slope (such as for the case of cristobalite, outlined in Fig. 9b), the way of treating the thermodynamics of the phase transition affects the calculated extrinsic stability limits of the polymorphs. In the adopted model the λtransition of cristobalite begins at T_{ref} = 298.15 K (at room pressure) and ends at $T_C \cong T_\lambda$ = 550 K. If the λ-contributions to the stability of the α polymorph were ignored, a first-order phase transition would be predicted already at T = 522 K, while, allowing T_λ to migrate with pressure according to the dT/dP slope of the phase boundary (i.e. 0.1217 K/bar; cf. Table 5), the transition at room pressure takes place correctly at T_λ = 550 K even though the Clapeyron slope is somewhat affected (i.e. dT/dP = 0.1131 K/bar). To avoid this problem (virtually negligible for all the other phases in this study) one should perform a complex VdP integration along the entire transition boundary. In practice this is not necessary and the transition may be treated as first-order (embodying the λ-contributions at the standard state into the $H°_f$, S_0, V_0 values). The inspection of the 2nd-order effect is however important to assess the correct thermal expansion of the low-T polymorph, as previously discussed. The assessment of thermodynamic and thermophysical properties of the low-density polymorphs of silica and the pure liquid allows to infer subsolidus phase relations and melting curves in the low-P range. The results of this calculation are shown in Fig. 10. The

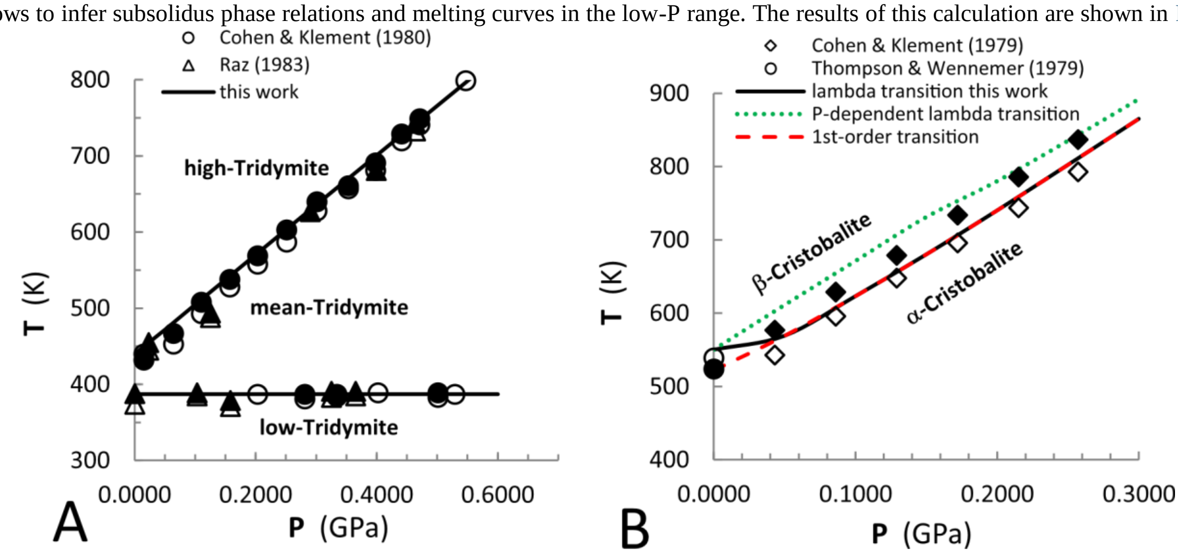

Fig. 9. Phase transitions in tridymite (A) and cristobalite (B) as compared with experimental observations [87,88,91,92] (full and empty symbols denote reversals). Black solid and red dashed curves in Fig. 9B represent the calculated phase boundary between α/β cristobalite by including or neglecting, respectively, λ-contributions to the stability of the α polymorph. Green dotted line is the result obtained by assuming T_λ to be pressure-dependent according to the Clapeyron slope of the phase boundary (i.e. dT/dT = 0.1217 K/bar) (see text for details). (For interpretation of the references to color in this figure legend, the reader is referred to the web version of this article.)

agreement with experimental observations [82,83,138–143] is reasonable. According to our assessment the βcrystobalite/β-quartz/liquid invariant point occurs at P = 0.48 GPa and T = 1990 K, while the high-tridymite/β-cristobalite/β-quartz invariant point is localized at P = 0.152 GPa and T = 1439 K (P = 0.151 GPa and T = 1440 K according to Berman [42]). A detailed tabulation of the thermodynamic properties of some the most relevant SiO_2 phases (solid polymorphs and liquid) at room pressure is proposed in Table 7.

4.2. The SiO_2 phase diagram at intermediate pressure

The assessed phase diagram of SiO_2 in the 1 GPa ≤ P ≤ 6 GPa range is shown in Fig. 11. The experimental observations concerning the univariant phase boundary between the α/β polymorphs of quartz and between β-quartz and coesite are sufficiently well reproduced as compared to the results of Cohen and Klement [82] and Mirwald and Massonne [83]. The α-quartz/coesite phase boundary is not far from the experimental observations of Bohlen and Boettcher [144] though we have no evidence of a constant Clapeyron slope, as inferred by different experimental investigations [82,83,144,145]. The β-quartz/ coesite/liquid invariant point is predicted to occur at P = 4.75 GPa and T ≅ 2630 K. The α-quartz/β-quartz/coesite invariant point is calculated at P = 3.3 GPa and T ≅ 1550 K (Fig. 11).

4.3. The SiO_2 phase diagram at high pressure

The high-pressure melting curves of coesite and stishovite are consistent with the experimental results of Dalton and Presnall [14],

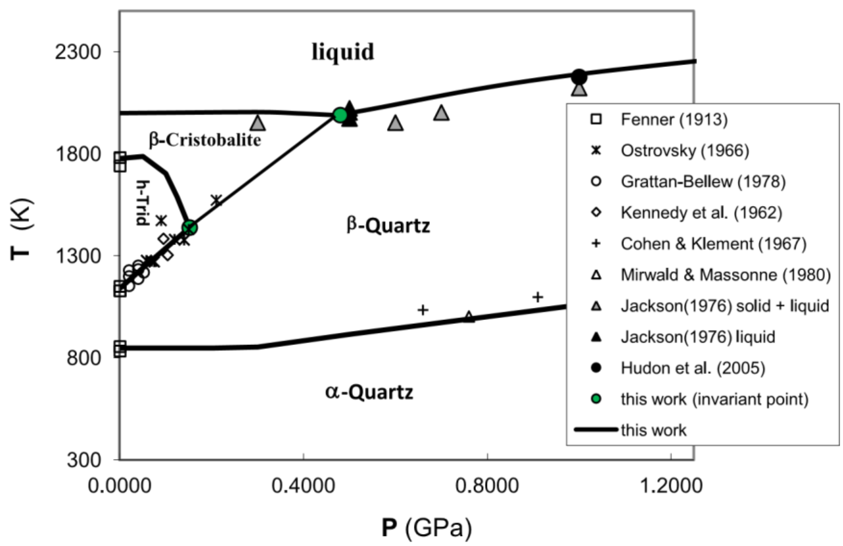

Fig. 10. SiO_2 phase diagram at low pressure (P ≤ 1.25 GPa). Melting curves and extrinsic stability limits of β-cristobalite, high-tridymite and the α, β polymorphs of quartz as obtained in this study (solid lines) are compared with experimental observations (symbols) [82,83,138–143].

Table 7

Thermodynamic and thermophysical properties of SiO_2 solid and liquid phases (T = 298.15 − 5000 K, P = 1 bar).

Polymorph	T	V	density	$\alpha\times10^6$	K	C_P	anharmonicity	H	S	G
	K	J/bar	g/cm^3	K−1	GPa	J/(mol×K)	J/(mol×K)	kJ/mol	J/(mol×K)	kJ/mol
α-Quartz	298.15	2.269	2.648	49.765	38.5	44.742	0.645	−910.700	41.460	−923.061
α-Quartz	300	2.269	2.648	49.640	38.5	44.935	0.646	−910.617	41.737	−923.138
α-Quartz	400	2.280	2.635	42.884	38.0	53.526	0.637	−905.665	55.925	−928.035
α-Quartz	500	2.290	2.624	36.128	37.5	59.495	0.560	−899.999	68.543	−934.270
α-Quartz	600	2.302	2.610	29.372	37.0	64.490	0.440	−893.797	79.836	−941.699
α-Quartz	700	2.320	2.590	22.616	36.5	69.645	0.301	−887.096	90.156	−950.205
α-Quartz	800	2.347	2.560	15.860	36.0	75.750	0.167	−879.836	99.842	−959.709
α-Quartz	848	2.367	2.538	12.617	35.8	70.200	0.112	−876.119	104.352	−964.610
Δ		0.018	−0.019					0.499	0.589	
β-Quartz	848	2.385	2.519	−5.936	57.9	67.632	0.041	−875.620	104.941	−964.611
β-Quartz	900	2.384	2.520	−6.300	54.8	68.296	0.047	−872.086	108.986	−970.174
β-Quartz	1000	2.382	2.522	−7.000	49.4	69.356	0.058	−865.201	116.239	−981.440
β-Quartz	1100	2.381	2.524	−7.700	44.6	70.203	0.069	−858.222	122.891	−993.401
β-Quartz	1139	2.380	2.525	−7.973	42.9	70.489	0.074	−855.478	125.341	−998.242
Δ		0.377	−0.345			0.937	−0.074	2.076	1.821	0.002
high-Tridymite	1139	2.757	2.179	−0.179	30.8	71.426	0.000	−853.402	127.162	−998.240
high-Tridymite	1200	2.757	2.179	−1.866	30.8	71.787	0.004	−849.034	130.898	−1006.112
high-Tridymite	1300	2.756	2.180	−4.631	30.8	72.281	0.024	−841.830	136.665	−1019.494
high-Tridymite	1400	2.754	2.182	−7.397	30.8	72.679	0.065	−834.581	142.036	−1033.432
high-Tridymite	1500	2.752	2.183	−10.162	30.8	73.006	0.131	−827.296	147.062	−1047.889
high-Tridymite	1600	2.749	2.186	−12.928	30.8	73.277	0.226	−819.982	151.783	−1062.834
high-Tridymite	1700	2.745	2.189	−15.693	30.8	73.503	0.354	−812.642	156.232	−1078.237
high-Tridymite	1767	2.742	2.191	−17.546	30.8	73.635	0.459	−807.713	159.076	−1088.800
Δ		0.005	−0.004			0.226	−0.433	0.123	0.069	
β-Cristobalite	1767	2.747	2.187	−7.114	10.5	73.861	0.026	−807.590	159.145	−1088.800
β-Cristobalite	1800	2.746	2.188	−7.687	10.4	73.968	0.030	−805.151	160.513	−1094.074
β-Cristobalite	1900	2.744	2.190	−9.423	10.2	74.227	0.047	−797.739	164.520	−1110.327
β-Cristobalite	1999	2.741	2.192	−11.141	10.0	74.550	0.068	−790.372	168.300	−1126.803
Δ		0.055	−0.043			7.123	−0.027	9.009	4.517	

Liquid	1999	2.796	2.149	12.126	5.0	81.673	0.041	−781.363	172.817	−1126.824
Liquid	2000	2.797	2.148	12.090	5.0	81.674	0.041	−781.281	172.858	−1126.997
Liquid	2500	2.801	2.145	−5.965	5.0	82.486	0.012	−740.242	191.170	−1218.166
Liquid	3000	2.780	2.161	−24.020	5.0	83.431	0.241	−698.772	206.289	−1317.639
Liquid	3500	2.734	2.198	−42.075	5.0	84.631	0.847	−656.768	219.236	−1424.095
Liquid	4000	2.665	2.255	−60.130	5.0	86.142	1.927	−614.089	230.632	−1536.617
Liquid	4500	2.575	2.333	−78.185	5.0	87.997	3.541	−570.569	240.882	−1654.537
Liquid	5000	2.465	2.438	−96.240	5.0	90.216	5.708	−526.031	250.265	−1777.355

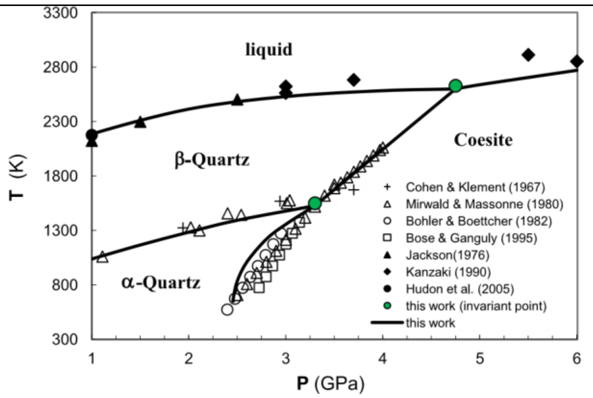

Fig. 11. SiO_2 phase diagram at intermediate pressure (1 GPa ≤ P ≤ 6 GPa). Melting curves and extrinsic stability limits of coesite and the α, β polymorphs of quartz as obtained in this study (solid lines) are compared with experimental observations (symbols) [82,83,143–146].

Shen and Lazor [15] and Kanzaki [146] (Fig. 12). The calculated univariant phase boundary between coesite and stishovite reproduces satisfactorily the observations of Akaogi et al. [54,56] and Zhang et al. [147,148]. The coesite/stishovite/liquid invariant point is predicted to occur at P = 13.8 GPa and T = 3177 K.

4.4. The Ca_2SiO_4 orthosilicate phase diagram

The phase diagram of Ca_2SiO_4 calculated up to P = 30 GPa is shown in Fig. 13. γ-Ca_2SiO_4 (Ca-olivine) is the stable polymorph at ambient

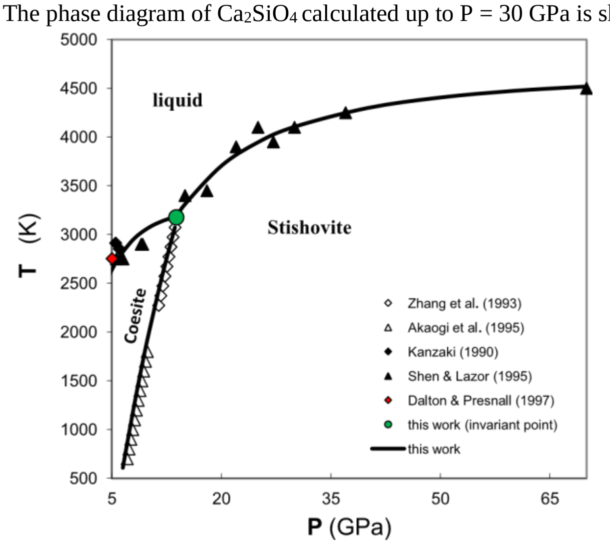

Fig. 12. SiO_2 phase diagram at high pressure (5 GPa ≤ P ≤ 70 GPa). Melting curves and extrinsic stability limits of coesite and stishovite as obtained in this study (solid lines) are compared with experimental observations (symbols) [14,15,56,146,147].

conditions. The γ/β phase transition has a negative Clapeyron slope, while both the α/α' and α'/β transitions are progressively shifted to higher T with the increasing pressure. The α/α', α'/β and γ/β univariant phase boundaries are more or less consistent with Remy et al. [149]. The α'/β univariant curve matches the phase transition detected by Wang and Weidner [150] at ~9 GPa and 1350 K. α' is the

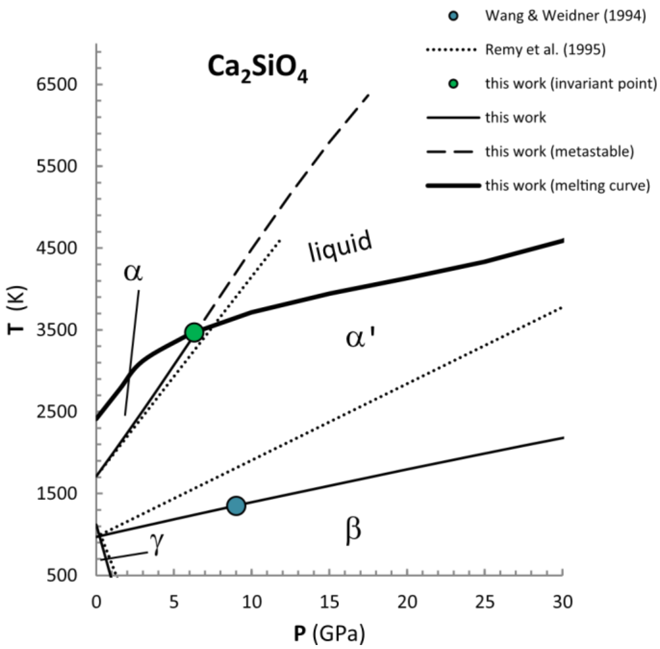

Fig. 13. Computed phase diagram of Ca_2SiO_4. The α/α', α'/β and γ/β univariant phase boundaries are consistent with experimental results and previous assessments [149,150].

stable polymorph at liquidus above ~6.3 GPa. A nearly similar diagram, though limited to subsolidus conditions, was recently proposed by Xiong et al. [151]. The α'/α/liquid invariant point occurs at P = 6.3 GPa and T ≅ 3470 K. The invariant point γ/β/α' at subsolidus is localized at P = 0.2 GPa and T ≅ 980 K.

4.5. The $CaSiO_3$ metasilicate phase diagram

The calculated phase diagram of $CaSiO_3$ is shown in Fig. 14 as compared with different experimental results [105,108,116,125,132, 143,152–155] in the P range from 1 bar to 16 GPa. The overall agreement is satisfactory. Subsolidus phase boundaries at low pressure (i.e. P ≤ 3 GPa) are consistent with the data of Kushiro [105], Huckenholz and Yoder [153], Essene [108] and Chatterjee et al. [116]. The Clapeyron slope of the pseudowollastonite to wollastonite

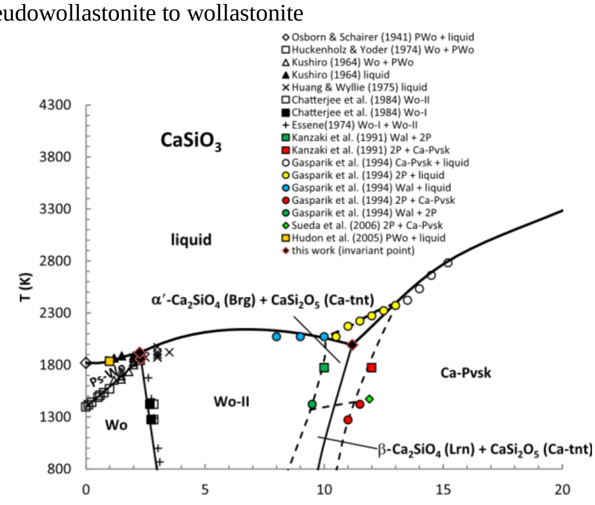

Fig. 14. Computed phase diagram of $CaSiO_3$. Thin and bold solid lines indicate the stability limits at subsolidus and the high-pressure melting curves of the solid polymorphs, respectively. Selected experimental data [105,108,116,125,132,143,152– 155] are also shown for comparison (symbols). Black diamonds indicate true invariant points. The dotted lines at liquidus and subsolidus conditions locate the Ca_2SiO_4 + $CaSi_2O_5$ two-phase field replacing that of $CaSiO_3$ (Wo-II) in a limited P-T range.

phase boundary as obtained in this work (i.e. 0.0049 GPa/K) is consistent with the experimental values, ranging from 0.0048 GPa/K to 0.0057 GPa/K [105,153,154]. The wollastonite to wollastonite-II phase boundary has a negative slope (i.e. −0.00063 GPa/K) which is consistent with previous experimental findings (ranging from −0.00047 GPa/K to −0.00084 GPa/K; [108,116,154]) and quite different from that inferred by calorimetric data (ranging from −0.0015 GPa to −0.0024 GPa/K, [131]). The calculated melting point of $CaSiO_3$ at 1bar pressure (i.e. 1820 K) matches the experimental value of Osborn and Schairer [152]. To reproduce the liquidus at high pressure we introduced a small excess volume in the liquid (Table 5; see also Sections 4.7. and 5), in a quite similar way to what inferred by us for the MgO-SiO_2 binary system [7]. The high-pressure melting curves calculated in this work for the $CaSiO_3$ polymorphs are in agreement with the experimental data of Kushiro [105] and Gasparik et al. [125], while Huang and Wyllie [154] give slightly lower melting temperatures for wollastonite-II (see Fig. 14). Pseudowollastonite is the stable polymorph at liquidus below ∼2 GPa, being replaced by wollastonite in a very narrow P range, and then by walstromite (wollastonite-II in our assessment) at P > 2.5–3 GPa (Fig. 14). In the pressure range between 8 and 10 GPa a disproportionation reaction of $CaSiO_3$ (Wo-II) to α'-Ca_2SiO_4 (bredigite) + $CaSi_2O_5$ (Ca-titanite) occurs [125,155], then the high-pressure polymorph of $CaSiO_3$ (Ca-perovskite) stabilizes at P > 10–13 GPa (see Fig. 14). The invariant points on the liquidus are observed at P = 2.25 GPa, T ≅ 1920 K (pseudowollastonite/wollastonite/liquid) and P = 11.18 GPa, T = 1994 K (wollastonite-II or walstromite/Ca-perovskite/liquid; metastable). The extension of the Ca_2SiO_4 + $CaSi_2O_5$ two-phase field detected by experiments is reproduced as well (thin dashed lines in Fig. 14).

4.6. The CaO-SiO_2 binary system at P = 1 bar

Although the CaO-SiO_2 system is one of the most studied in the literature, there is considerable disagreement as to the assessment of the CaO-rich side of the phase diagram [18,20–25]. As discussed, the uncertainty on the liquidus is mostly related to contradictory experimental results on the melting point of CaO. Thermodynamic assessments based on the modified quasichemical model turn out to be consistent with a melting point of lime around 2845 K [18,20–23], other assessments with a higher melting temperature (i.e. around ~3200 K) [24,25]. Our assessment, which is based on the first principles modeling of CaO solid and liquid phases (see Sections 2.1.2 and 2.1.3), is consistent with a T_f = 3202 K for lime, in close agreement with recent experimental data [28] and MD results [29]. The liquidus curve on the CaO-rich side of the phase diagram is thus shifted to higher temperatures, but this is not in contrast and compatible with experimental observations both at 1-bar and highpressure conditions (see Fig. 15A and B).

According to our assessment at 1-bar pressure the CaO-SiO_2 system has two congruently melting compounds (the orthosilicate Ca_2SiO_4 and the metasilicate $CaSiO_3$) and two incongruently melting compounds (Ca_3SiO_5 hatrurite and $Ca_3Si_2O_7$ rankinite) (Fig. 15A and Table 8). The stable polymorph of Ca_2SiO_4 at liquidus is α-larnite, which melts at T = 2404 K, in close agreement with experimental observations [156–158]. Rankinite ($Ca_3Si_2O_7$) melts incongruently to form larnite (α-Ca_2SiO_4) plus liquid at T = 1750 K. The peritectic point (liquid + α-Ca_2SiO_4 = $Ca_3Si_2O_7$) calculated in this work at X_{SiO2} = 0.41 ± 0.01 compares fairly well with the experiments of Rankin and Wright [159] and Osborn [156], who detected peritectic melting of rankinite at T = 1748 ± 5 K,
X_{SiO2} = 0.428 and T = 1737 K, X_{SiO2} = 0.431, respectively. A slightly lower silica content with respect to experiments is thus inferred for this peritectic point, as already pointed out by other thermodynamic assessments: Hillert et al. [24] give T = 1751 K and X_{SiO2} = 0.409; Hillert et al. [160] give T = 1745 K and X_{SiO2} = 0.409, after a reevaluation of thermodynamic properties of rankinite; Eriksson et al. [18] give T = 1737 ± 10 K and X_{SiO2} = 0.41 ± 0.01. Rankinite

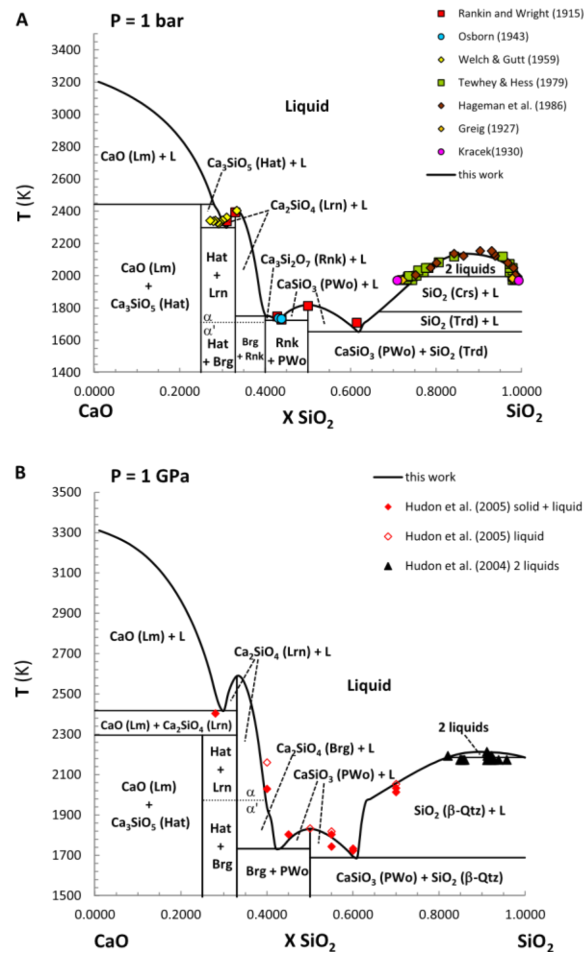

Fig. 15. Melting relations in the CaO-SiO_2 binary system. (A) P = 1 bar; (B) P = 1 GPa. Experimental observations (symbols) at 1 bar [156,157,159,169–172] and 1 GPa [143,175] are superimposed for comparative purposes. Thin dotted lines locate the α/ α' phase transition of Ca_2SiO_4 at subsolidus conditions.

forms an eutectic with $CaSiO_3$ pseudowollastonite at T = 1724 K and X_{SiO2} = 0.43, in agreement with experimental findings [156,159]. The calculated melting point of $CaSiO_3$ pseudowollastonite at 1-bar pressure is 1820 K, which is consistent with the value given by Osborn and Schairer [152] (i.e. 1821 K). Some discrepancy exists as to the eutectic point between $CaSiO_3$ (pseudowollastonite) and SiO_2 (high-tridymite), which is predicted to occur at T = 1653 K and X_{SiO2} = 0.62 by our modeling, while experimental works locate this point at T = 1709 K and X_{SiO2} = 0.614–0.624 [156,159].

The melting behavior of hatrurite (Ca_3SiO_5) is highly controversial and deserves special attention. The key point is as to whether this compound is stable on the liquidus (or solidus) of the CaO-SiO_2 binary system [157,158,161] or decomposes into a mixture of lime and larnite before melting conditions are reached [159,162–164]. In this work we assumed as valid the critical considerations made on literature results by Welch and Gutt [157], who pointed out the possible reasons why the observation of the narrow primary crystallization field of Ca_3SiO_5 could be easily lost during quenching experiments. Furthermore, it is noteworthy that hatrurite is observed as primary phase in the CaOAl_2O_3-SiO_2 and CaO-MgO-SiO_2 ternary systems [159,165,166]. A peritectic point between lime and hatrurite (i.e. liquid + CaO = Ca_3SiO_5) and a eutectic point between hatrurite and α-larnite (i.e. liquid = Ca_3SiO_5 + Ca_2SiO_4) are thus calculated in this work at T = 2443 K, X_{SiO2} = 0.28 ± 0.01 and T = 2298 K, X_{SiO2} = 0.31 ± 0.01, respectively, by adjusting the $H°_{f,298}$ value of hatrurite by − 5600 J/mol with respect to the tabulation of Haas et al. [100]. This change is within the range of experimental uncertainty, since $H°_{f,298}$ of this compound differs by more than 14,000 J/mol among different compilations [31,99,100,118,167]. The calculated invariant points of Ca_3SiO_5 are in agreement both with experiments [157,158] and the results of a number of assessments [24,25,160,166,168] (see Table 8). The thermodynamic and thermophysical properties optimized in this work for this compound also allow to obtain meaningful stability relations at high-pressure conditions (see Section 4.7).

The topology of the liquid-liquid miscibility gap calculated at ambient pressure on the SiO_2-rich side of the binary system is consistent with the observations of Tewhey and Hess [169] and Hageman et al. [170] (Fig. 15A) and it extends from the nearly pure silica composition to X_{SiO2} = 0.76 at P = 1 bar. The calculated monotectic temperature is T = 1994 K, which is closer to the value inferred by Hageman et al. [170] (i.e. T = 2005 K at X_{SiO2} = 0.752) and slightly higher than those determined by less recent experimental works (i.e. T = 1971 K at X_{SiO2} = 0.71–0.72, [169,171–173]; see also [174] for a review of experimental results). The consolute point is predicted to occur at T = 2137 K and X_{SiO2} = 0.87 ±

0.01, in overall agreement with the experimental determinations of Tewhey and Hess [169] (T = 2144 K and X_{SiO2} = 0.91 ± 0.01) and Hageman et al. [170] (T = 2159 ± 1 K and X_{SiO2} = 0.902).

4.7. The effect of pressure on the CaO-SiO_2 binary system

The calculated CaO-SiO_2 phase diagram at P = 1 GPa is shown in Fig. 15B. As expected, the increase of pressure induces an upward shift of the liquidus. At P = 1 GPa the topology of the phase diagram simplifies since Ca_3SiO_5 (hatrurite) and $Ca_3Si_2O_7$ (rankinite) are no more stable on the liquidus, and there are only three eutectic points. A first eutectic point between CaO (lime) and Ca_2SiO_4 (α-larnite) is predicted to occur at T = 2418 K and X_{SiO2} = 0.30, in good agreement with the pyston-cylinder experiments of Hudon et al. [143] (see Table 8). Larnite melts congruently at T = 2589 K at this pressure, then the liquidus curve steeply decreases up to T = 1733 K, where a second eutectic point between Ca_2SiO_4 (α'-bredigite) and $CaSiO_3$ (pseudowollastonite) occurs (Fig. 15B). So, Ca_2SiO_4 undergoes a phase transition at T = 1973 K, P = 1 GPa (Fig. 13) and the α'-polymorph stabilizes on the liquidus. Remy et al. [149] give a slightly lower temperature for the α-α' phase transition of Ca_2SiO_4 (i.e. T = 1954 K); Hudon et al. [143] a higher eutectic temperature between Ca_2SiO_4 and $CaSiO_3$ (i.e. T = 1760 K). The stable polymoph of $CaSiO_3$ at P = 1 GPa is still pseudowollastonite (Fig. 14), which melts congruently at T = 1832 K, in agreement with experimental results (i.e. T = 1826 ± 11 [143]; T = 1841 ± 15 [154]). Despite Ca_3SiO_5 is no more stable on the liquidus at P = 1 GPa, our assessment is consistent with its near-solidus stability at this pressure, since a decomposition reaction of lime and αlarnite to give hatrurite is predicted to occur at T = 2296 K (see Fig. 15B). This result is consistent with the experimental results of Hudon et al. [143], who found hatrurite + larnite + glass in their experimental run at T = 2373 ± 5 K, P = 1 GPa and hatrurite + larnite at T = 2053 ± 5 K, P = 1 GPa. However, these Authors do not provide any thermophysical parameters for hatrurite, so that this phase does not compare in their assessed phase diagram at P = 1 GPa (see Fig. 2b in Hudon et al. [143]). The thermodynamic and thermophysical properties optimized in this work for hatrurite provide consistent melting phase relations both at ambient and high-pressure conditions.

The liquid-liquid miscibility gap still survives at P = 1 GPa, though flattened and drastically reduced in width: the calculated monotectic temperature is only 28 K lower than the consolute temperature at this pressure (i.e. T = 2185 K vs. 2213 K). As already pointed out for the MgO-SiO_2 system [7], a negative excess volume seems to occur also in the CaO-SiO_2 liquid: this contribution, which is quite small at P = 1 GPa and quickly goes to zero with the increasing pressure (see Table 5 and Eqs. 9 and 10 in Section 3), is consistent with the experimental findings of Hudon and coworkers [143,175] (see Fig. 15B) and, in particular, with the disappearance of the liquid-liquid

Table 8
Calculated vs experimental invariant points (binary eutectics and peritectics) in the CaO-SiO_2 system at P = 1 bar and P = 1 GPa. Melting points of Ca_2SiO_4 and $CaSiO_3$ are also reported. Abbreviation for solid phases as in Figs. 14 and 15; L = liquid phase.

P = 1 bar				
Invariant point	CaO (Xmol)	SiO_2 (Xmol)	T (K)	Ref.
L + CaO (Lm) = Ca_3SiO_5 (Hat)	0.72	0.28	2443	(1)
	0.728 − 0.729	0.272 − 0.271	2423 − 2343	(2,3)[a]
	0.729 − 0.730	0.271 − 0.270	2391 − 2428	(4,5,6,7,8)[b]
L = Ca_2SiO_4 (α-Lrn) + Ca_3SiO_5 (Hat)	0.69	0.31	2298	(1)
	0.71	0.29	2323	(2,3)[a]
	0.698 − 0.705	0.302 − 0.295	2323 − 2333	(4,5,6,7,8)[b]
L + Ca_2SiO_4 (α-Lrn) = $Ca_3Si_2O_7$ (Rnk)	0.59	0.41	1750	(1)
	0.569 − 0.572	0.431 − 0.428	1737 − 1748	(9,10)[a]
	0.569 − 0.592	0.431 − 0.409	1732 − 1751	(5,6,7,8,11)[b]
L = $Ca_3Si_2O_7$ (Rnk) + $CaSiO_3$ (PWo)	0.57	0.43	1724	(1)
	0.562	0.438	1733 − 1728	(9,10)[a]
	0.565 − 0.580	0.435 − 0.420	1727 – 1733	(5,6,7,8,11)[b]
L = $CaSiO_3$ (PWo) + SiO_2 (Trd)	0.38	0.62	1653	(1)
	0.376 − 0.386	0.624 − 0.614	1709	(9,10)[a]
	0.368 − 0.392	0.632 − 0.608	1705 − 1715	(4,5,6,7,8,11)[b]
Melting point	CaO (Xmol)	SiO_2 (Xmol)	T (K)	Ref.
L = Ca_2SiO_4 (α-Lrn)	0.67	0.33	2404	(1)
	0.67	0.33	2403 − 2393	(2,3,9,10)[a]
	0.67	0.33	2403 − 2413	(5,6,7,8,11)[b]
L = $CaSiO_3$ (PWo)	0.50	0.50	1820	(1)
	0.50	0.50	1813 − 1821	(10,12)[a]
	0.50	0.50	1813 − 1817	(4,5,6,7,8,11)[b]
P = 1 GPa				
Invariant point	CaO (Xmol)	SiO_2 (Xmol)	T (K)	Ref.
L = CaO (Lm) + Ca_2SiO_4 (α-Lrn)	0.70	0.30	2418	(1)
	0.714	0.286	2428	(13)a,b
L = Ca_2SiO_4 (α'-Brg) + $CaSiO_3$ (PWo)	0.57	0.43	1733	(1)
	0.57	0.43	1760	(13)a,b
L = $CaSiO_3$ (PWo) + SiO_2 (β-Qtz)	0.39	0.61	1689	(1)
	0.40	0.60	1739	(13)a,b
Melting point	CaO (Xmol)	SiO_2 (Xmol)	T (K)	Ref.
L = Ca_2SiO_4 (α-Lrn)	0.67	0.33	2589	(1)
L = $CaSiO_3$ (PWo)	0.50	0.50	1832	(1)
	0.50	0.50	1826 ± 11	(13)a,b

This work (2) Gutt [158] (3) Welch and Gutt [157] (4) Blander and Pelton [168] (5) Taylor and Dinsdale [25]; (6) Hillert et al. [24]; (7) Hillert et al. [160]; (8) Huang et al. [166]; (9) Osborn [156]; (10) Rankin and Wright [159]; (11) Eriksson et al. [18]; (12) Osborn and Schairer [152]; (13) Hudon et al. [143].

a

Experimental data. b Thermodynamic assessment.

miscibility gap in the $CaO-SiO_2$ system at pressures between 1 and 2 GPa.

Fig. 16 depicts the evolution of the $CaO-SiO_2$ liquidus with pressure (from 1 bar to 25 GPa). The orthosilicate Ca_2SiO_4 persists to melt

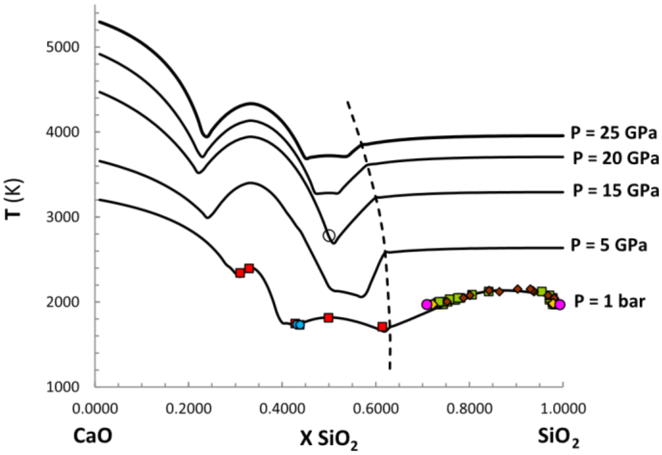

Fig. 16. Evolution of the $CaO-SiO_2$ liquidus with pressure (from 1 bar to 25 GPa). Experimental observations (symbols) are superimposed for comparative purposes. Symbols as in Fig. 15, except for Gasparik et al. [125] at P = 15 GPa (empty square). The dashed line indicates the limit of maximum depolymerization in the liquid at different pressures.

congruently at all investigated pressures, despite the structural rearrangements dictated by pressure (see Fig. 13 and Section 4.4). On the other hand, pressure effects change the melting behavior of the metasilicate $CaSiO_3$, which melts congruently as pseudowollastonite in the low-pressure range, then melts incongruently as wollastonite-II (or walstromite) in the intermediate-pressure range and finally again congruently as Ca-perovskite at higher pressures (Fig. 16). Those changes in the melting behavior of $CaSiO_3$ with pressure seem to be closely related to the complex polymorphism of this phase (cf. Fig. 14 and Section 4.5).

Ca_2SiO_4 is an efficient thermal barrier in the whole investigated range and it forms two invariant points (eutectics or peritectics) with CaO (on the left-hand side of the phase diagram) and $CaSiO_3$ (on the right-hand side), except for a narrow pressure range between ~10 and 15 GPa where the metasilicate is no more stable on the liquidus and the two-phase assemblage Ca_2SiO_4 (α'-bredigite first, then β-larnite) + $CaSi_2O_5$ (Ca-titanite), instead of $CaSiO_3$, becomes stable (Fig. 14).

Pressure effects change also the composition of the main invariant points in the $CaO-SiO_2$ system, but in complex way (Fig. 16). The composition of the eutectic point between CaO (lime), Ca_2SiO_4 (αlarnite or α'-bredigite) and liquid shifts from $X_{SiO2} = 0.30$ at P = 1 GPa (and T = 2418 K) to $X_{SiO2} = 0.22$ at P =10 GPa (and T = 3321 K), then its silica content slowly increases again up to $X_{SiO2} = 0.24$ at P = 25 GPa (and T = 3945 K). The same trend occurs in the eutectic between $CaSiO_3$, SiO_2 and liquid: the silica content of this eutectic lowers with the increasing pressure, from $X_{SiO2} = 0.62$ at P = 1 bar to $X_{SiO2} = 0.49$ at P = 18 GPa, then increases again up to $X_{SiO2} = 0.53$ in the pressure range 18 GPa < P < 25 GPa. In this case, the change of the eutectic composition seems to be independent from the solid-state polymorphism of $CaSiO_3$ (stable on the liquidus as pseudowollastonite, wollastonite-II and Ca-perovskite at low-, intermediate- and high-pressure conditions, respectively; see Fig. 14). Melting phase relations of the Ca_2SiO_4-$CaSiO_3$ join are even more complex. In the low-pressure range (i.e. up to P ≅ 4 GPa) an eutectic point between α-larnite and pseudowollastonite, α'-bredigite and pseudowollastonite or α'-bredigite and wollastonite-II is progressively enriched in SiO_2 with the increasing pressure. Then melting of $CaSiO_3$ (Wo-II) becomes incongruent and a peritectic point between α'-bredigite, wollastonite-II and liquid occurs along the join. This peritectic is displaced towards the SiO_2 compositional limit of the system until pressure effects stabilize a congruently melting polymorph of $CaSiO_3$, namely Ca-perovskite, and a novel eutectic point between α'-bredigite and Ca-perovskite appears in the system (Fig. 16). Also in this case, an inversion occurs in the compositional trend of the eutectic point, since its composition becomes progressively enriched in CaO at P > 15 GPa (i.e. from $X_{SiO2} = 0.49$ at P = 18 GPa T = 3052 K to $X_{SiO2} = 0.45$ at P = 25 GPa, T = 3691 K).

As already pointed out, the liquid-liquid miscibility gap in the $CaOSiO_2$ system progressively shrinks with the increasing pressure, up to disappear between 1 and 2 GPa (Figs. 15 and 16). The attainment of the limit of maximum depolymerization in the liquid produces a kink in the liquidus curve on the SiO_2-rich side of the phase diagram (see dashed line in Fig. 16) which is possibly a numerical artifact produced by the Gibbs free energy minimization procedure (see Supplementary material for details).

5. Conclusions

Thermodynamic assessment and phase diagram calculation at high pressure and temperature must be assisted by stringent guidelines. The combination of thermodynamic and thermophysical properties of liquid and solid phases requires, whenever possible, first principles data or, at least, some theoretically grounded criteria to avoid physical unsoundness. In this work an ab initio-assisted and comprehensive assessment of the $CaO-SiO_2$ system in the pressure range from P = 1 bar to P = 25 GPa have been accomplished according to the following guidelines:

i) the high-T extrapolation of the isobaric heat capacity must be consistent with the Dulong-Petit asymptotic limit (i.e. 3nR + $T V \alpha_V^2 K_T$); ii) any form of thermodynamic assumption not based on the Gibbs free energy minimization principle must be avoided: the adopted heat capacity functions cannot thus have any apparent discontinuity within the intrinsic stability field of any substance nor P-T limitations may be imposed within the investigated range of physical conditions. It follows from this criterion that any apparent stability of a given solid polymorph outside its well-established stability field is indicative of physical unsoundness in the adopted thermodynamic or thermophysical parameterization;

iii) in the assessment of polymorphic phase transitions over a widethermobaric regime, the limited range of experimental observations and the necessity of providing thermophysical data valid for the entire P-T realm of interest could limit the choice of appropriate thermal expansion and compressibility data. In other terms, a close fit of discrete experimental data performed in a restricted Trange could result in aberrant progressions outside the limits of interpolation. For these reasons, the definition of a "lattice" heat capacity (according to Berman and coworkers, [42,69,70]), on which the effects of λ-type or 1st-order phase transitions are eventually superimposed, could be beneficial along with the use of criterion i);

iv) the combined use of first principles Polarized Continuum Model calculations for the pure CaO and SiO_2 liquid oxides and the Hybrid Polymeric Approach for the binary liquid phase prove to be a powerful tool in the assessment of melting phase relations;

v) the adoption of ab initio thermodynamic properties calculated for some key solid phases (like CaO lime and SiO_2 stishovite) may act as cornerstone in the subsequent physically-consistent assessment of phase diagrams at high pressure and temperature conditions.

Appendix A. Supplementary material

Supplementary data associated with this article can be found in the online version at http://dx.doi.org/10.1016/j.calphad.2017.07.009.

References

[1] M. Vetuschi Zuccolini, G. Ottonello, D. Belmonte, Ab-initio assessment of conventional standard-state thermodynamic properties for geochemically relevant gaseous and aqueous species, Comput. Geosci. 37 (2011) 646–661.

[2] D. Belmonte, G. Ottonello, M. Vetuschi Zuccolini, Melting of α-Al_2O_3 and vitrification of the undercooled alumina liquid: Ab initio vibrational calculations and their thermodynamic implications, J. Chem. Phys. 138 (2013) 064507. http://dx.doi.org/10.1063/1.4790612.

[3] J. Tomasi, M. Persico, Molecular interactions in solution: an overview of methods based on continuous distributions of the solvent, Chem. Rev. 94 (1994) 2027–2094.

[4] C. Gatti, G. Ottonello, P. Richet, Energetics and bonding in aluminosilicate ring with alkali metal and alkaline-earth metal charge-compensating cations, J. Phys. Chem. A 116 (2012) 8584–8598.

[5] G. Ottonello, P. Richet, The solvation radius of silicate melts based on the solubility of noble gases and scaled particle theory, J. Chem. Phys. 140 (2014) 044506. http://dx.doi.org/10.1063/1.4862737.

[6] G. Ottonello, P. Richet, M. Vetuschi Zuccolini, The wet solidus of silica: predictions from the scaled particle theory and polarized continuum model, J. Chem. Phys. 142 (2015) 054503. http://dx.doi.org/10.1063/1.4906745.

[7] D. Belmonte, G. Ottonello, M. Vetuschi Zuccolini, M. Attene, The system $MgOAl_2O_3$-SiO_2 under pressure: a computational study of melting relations and phase diagrams, Chem. Geol. 461 (2017) 54–64. http://dx.doi.org/10.1016/j.chemgeo.2016.11.011.

[8] R. Jeanloz, T.J. Ahrens, H.K. Mao, P.M. Bell, B1-B2 transition in calcium oxide from shock-wave and diamond-cell experiments, Science 206 (1979) 829–830.

[9] B.B. Karki, R.M. Wentzcovitch, Vibrational and quasi-harmonic thermal properties of CaO under pressure, Phys. Rev. B 68 (2003) 224304.

[10] P.J. Heaney, Structure and chemistry of the low-pressure silica polymorphs, in: P.J. Heaney, C.T. Prewitt, G.V. Gibbs (Eds.), , Silica: Physical Behavior, Geochemistry and Materials Applications, Reviews in Mineralogy 29, Mineralogical Society of America, Chantilly, 1994, pp. 1–40.

[11] R.J. Hemley, J. Badro, D.M. Teter, Polymorphism in crystalline and amorphous silica at high pressures, in: H. Aoki, Y. Syono, R.J. Hemley (Eds.), Physics Meets Mineralogy, Cambridge University Press, New York, 2000, pp. 173–204.

[12] G. Ottonello, M. Vetuschi Zuccolini, D. Belmonte, The vibrational behaviour of silica clusters at the glass transition: ab initio calculations and thermodynamic implications, J. Chem. Phys. 133 (2010) 104508. http://dx.doi.org/10.1063/ 1.3483195.

[13] G. Ottonello, M. Attene, D. Ameglio, D. Belmonte, M. Vetuschi Zuccolini, M. Natali, Thermodynamic investigation of the CaO-Al_2O_3-SiO_2 system at high P and T through polymer chemistry and convex-hull techniques, Chem. Geol. 346 (2013) 81–92.

[14] J.A. Dalton, D.C. Presnall, No liquid immiscibility in the system $MgSiO_3$-SiO_2 at 5.0 GPa, Geochim. Cosmochim. Acta 61 (1997) 2367–2373.

[15] G. Shen, P. Lazor, Measurement of melting temperatures of some minerals under lower mantle pressures, J. Geophys. Res. – Solid Earth 100 (1995) 17699–17713. [16] S.K. Bajgain, D.B. Ghosh, B.B. Karki, First-principles simulations of CaO and $CaSiO_3$ liquids: structure, thermodynamics and diffusion, Phys. Chem. Miner. 42 (2015) 393–404.

[17] M.W. Chase {C}Jr., NIST-JANAF Thermochemical Tables, Journal of Physical and Chemical Reference Data. Monograph No. 9, fourth ed., American Chemical Society, American Institute of Physics and National Institute of Standards and Technology, New York.

[18] G. Eriksson, P. Wu, M. Blander, A.D. Pelton, Critical evaluation and optimization of the thermodynamic properties and phase diagrams of the MnO–SiO_2 and CaO– SiO_2 systems, Canad. Metall. Quart. 33 (1994) 13–21.
[19] J.F. Elliott, M. Gleiser, Thermochemistry for Steelmaking, Addison-Wesley, Boston, 1960.
[20] G. Eriksson, A.D. Pelton, Critical evaluation and optimization of the thermodynamic properties and phase diagrams of the CaO-Al_2O_3, Al_2O_3-SiO_2 and CaOAl_2O_3-SiO_2 systems, Metall. Trans. 24B (1993) 807–816.
[21] P. Wu, G. Eriksson, A.D. Pelton, Critical evaluation and optimization of the thermodynamic properties and phase diagrams of the CaO–FeO, CaO–MgO, CaO–MnO, FeO–MgO, FeO–MnO, and MgO–MnO systems, J. Am. Ceram. Soc. 76 (1993) 2065–2075.
[22] I.-H. Jung, S.A. Decterov, A.D. Pelton, Critical thermodynamic evaluation and optimization of the MgO-Al_2O_3, CaO-MgO-Al_2O_3, and MgO-Al_2O_3-SiO_2 systems, JPEDAV 25 (2004) 329–345.
[23] I.-H. Jung, S.A. Decterov, A.D. Pelton, Critical thermodynamic evaluation and optimization of the CaO–MgO–SiO_2 system, J. Eur. Ceram. Soc. 25 (2005) 313–333.
[24] M. Hillert, B. Sundman, X. Wang, An assessment of the CaO-SiO_2 system, Metall. Trans. 21B (1990) 303–312.
[25] J.R. Taylor, A.T. Dinsdale, Thermodynamic and phase diagram data for the CaOSiO_2 system, CALPHAD 14 (1990) 71–88.
[26] J.P. Traverse, M. Foex, Investigation of the ZrO_2–CaO, and ZrO_2–SrO systems, High Temp. High Press. 1 (1969) 409–427.
[27] T. Yamada, M. Yoshimura, S. Somiya, Reinvestigation of the solidification point of CaO by digital pyrometry, J. Am. Ceram. Soc. 69 (1986) C243–C245.
[28] D. Manara, R. Böhler, L. Capriotti, A. Quaini, Z. Bao, K. Boboridis, L. Luzzi, A. Janssen, P. Pöml, R. Eloirdi, R.J.M. Konings, On the melting behaviour of calcium monoxide under different atmospheres: a laser heating study, J. Eur. Ceram. Soc. 34 (2014) 1623–1636.
[29] X.W. Sun, T. Song, Y.D. Chu, Z.J. Liu, Z.R. Zhang, Q.F. Chen, The high-pressure melting curve of CaO, Solid State Comm. 150 (2010) 1785–1788.
[30] R.G. Berman, T.H. Brown, H.J. Greenwood, An internally consistent thermodynamic data base for minerals in the system Na_2O-K_2O-CaO-MgO-FeO-Fe_2O_3-Al_2O_3-SiO_2-TiO_2-H_2O-CO_2, University of British Columbia, Canada Atomic Energy Canada Ltd. Tech. Rep. 377 (1985).
[31] I. Barin, Thermochemical Data of Pure Substances, VCH, Weinheim, 1995.
[32] A.D. Becke, Density functional theochemistry. III The role of exact exchange, J. Chem. Phys. 98 (1993) 5648–5652.
[33] R. Dovesi, V.R. Saunders, C. Roetti, R. Orlando, C.M. Zicovich-Wilson, F. Pascale, B. Civalleri, K. Doll, N.M. Harrison, I.J. Bush, Ph D'Arco, M. Llunell, M. Causà, Y. Noël, CRYSTAL14 User's Manual, Università di Torino, Torino, 2014.
[34] D.H. Saunderson, G.E. Peckham, The lattice dynamics of calcium oxide, J. Phys. C 4 (1971) 2009–2016.
[35] G. Ottonello, B. Civalleri, J. Ganguly, W.F. Perger, D. Belmonte, M. Vetuschi Zuccolini, Thermo-chemical andthermo-physical properties of the highpressure phase anhydrous B ($Mg_{14}Si_5O_{24}$): an ab-initio all-electron investigation, Am. Mineral. 95 (2010) 563–573.
[36] D. Belmonte, G. Ottonello, M. Vetuschi Zuccolini, Ab initio thermodynamic and thermophysical properties of sapphirine end-members in the join $Mg_4Al_8Si_2O_{20}$ – $Mg_3Al_{10}SiO_{20}$, Am. Miner. 99 (2014) 1449–1461.
[37] D. Belmonte, C. Gatti, G. Ottonello, P. Richet, M. Vetuschi Zuccolini, Ab initio thermodynamic and thermophysical properties of sodium metasilicate, Na_2SiO_3, and their electron-density and electron-pair-density conunterparts, J. Phys. Chem. A 120 (2016) 8881–8895. http://dx.doi.org/10.1021/acs.jpca.6b08676.
[38] A. Erba, M. Shahrokhi, R. Moradian, R. Dovesi, On how differently the quasiharmonic approximation works for two isostructural crystals: thermal properties of periclase and lime, J. Chem. Phys. 142 (2015) 044114. http://dx.doi.org/ 10.1063/1.4906422.
[39] R.A. Robie, B.S. Hemingway, Thermodynamic Properties of Minerals and Related Substances at 298.15 K and 1 bar (10^5 Pa) Pressure and at Higher Temperatures 2131, U.S. Geological Survey Bullettin, Washington, 1995.
[40] Y. Th. Demuth, J. Jeanvoine, J.G. Hafner, Angyan, Polymorphism in silica studied in the local density and generalized-gradient approximations, J. Phys. Condens. Matter 11 (1999) 3833–3874.
[41] G. Ottonello, M. Vetuschi Zuccolini, B. Civalleri, Thermo-chemical and thermophysical properties of stishovite: an ab-initio all-electron investigation, CALPHAD 33 (2009) 457–468.
[42] R.G. Berman, Internally-consistent thermodynamic data for minerals in the system Na_2O-K_2O-CaO-MgO-FeO-Fe_2O_3-Al_2O_3-SiO_2-TiO_2-H_2O-CO_2, J. Petrol. 29 (1988) 445–522.
[43] M. Marsman, J. Paier, A. Stroppa, G. Kresse, Hybrid functionals applied to extended systems, J. Phys.: Condens. Matter 20 (2008) 064201.
[44] W.A. Bassett, J.D. Barnett, Isothermal compression of stishovite and coesite up to 85 kilobars at room temperature by x-ray diffraction, Phys. Earth Planet. Int. 3 (1970) 54–60.
[45] H. Ito, K. Kawada, S. Akimoto, Thermal expansion of stishovite, Phys. Earth Planet. Int. 8 (1974) 277–281.
[46] M. Sugiyama, S. Endo, K. Koto, The crystal structure of stishovite under pressure up to 6 GPa, Mineral. J. 13 (1987) 455–466.
[47] N.L. Ross, J.F. Shu, R.M. Hazen, T. Gasparik, High-pressure crystal chemistry of stishovite, Am. Mineral. 75 (1990) 739–747.
[48] B.S. Li, S.M. Rigden, R.C. Liebermann, Elasticity of stishovite at high pressure, Phys. Earth Planet. Int. 96 (1996) 113–127.

[49] V.V. Brazhkin, L.E. McNeil, M. Grimsditch, N.A. Bendeliani, T.I. Dyuzheva, L.M. Lityagina, Elastic constants of stishovite up to its amorphization temperature, J. Phys.: Condens. Matter 17 (2005) 1869–1875.
[50] M. De. La Pierre, D. Belmonte, Ab initio investigation of majorite and pyrope garnets: lattice dynamics and vibrational spectra, Am. Mineral. 101 (2016) 162–174.
[51] B. Olinger, The compression of stishovite, J. Geophys. Res. – Solid Earth 81 (1976) 5341–5343.
[52] J. Liu, J. Zhang, L. Flesh, B. Li, D.J. Weidner, D. Liebermann, Thermal equation of state of stishovite, Phys. Earth Planet. Int. 112 (1999) 257–266.
[53] J.L. Holm, O.L. Kleppa, E.F. Westrum, Thermodynamics of polymorphic transitions in silica. Thermal properties from 5 to 1070 °K and pressure-temperature stability fields for coesite and stishovite, Geochim. Cosmochim. Acta 31 (1967) 2289–2307.
[54] M. Akaogi, M. Oohata, H. Kojitani, H. Kawaji, Thermodynamic properties of stishovite by low-temperature heat capacity measurements and the coesitestishovite transition boundary, Am. Mineral. 96 (2011) 1325–1330.
[55] W. Yong, E. Dachs, A. Benisek, R.A. Secco, Heat capacity, entropy and phase equilibria of stishovite, Phys. Chem. Miner. 39 (2012) 153–162.
[56] M. Akaogi, H. Yusa, K. Shiraishi, T. Suzuki, Thermodynamic properties of αquartz, coesite and stishovite and equilibrium phase relations at high pressures and high temperatures, J. Geophys. Res. – Solid Earth 100 (1995) 22337–22347.
[57] H. Mao, B. Sundman, Z. Wang, S.K. Saxena, Volumetric properties and phase relations of silica – thermodynamic assessment, J. Alloy. Compd. 327 (2001) 253–262.
[58] J.R. Smyth, J.V. Smith, G. Artioli, Å. Kvick, Crystal structure of coesite, a highpressure form of SiO_2, at 15 and 298 K from single-crystal neutron and X-ray diffraction data: test of bonding models, J. Phys. Chem. 91 (1987) 988–992.
[59] K.L. Geisinger, M.A. Spackman, G.V. Gibbs, Exploration of structure, electron density distribution, and bonding in coesite with Fourier and pseudo atom refinement methods using single-crystal X-ray diffraction data, J. Phys. Chem. 91 (1987) 3237–3244.
[60] A. Kirfe, G. Will, J. Arndt, A new phase of coesite SiO_2, Z. Krist. 149 (1979) 315–326.
[61] L. Levien, C.T. Prewitt, High-pressure crystal structure and compressibility of coesite, Am. Mineral. 66 (1981) 324–333.
[62] E. Bourova, P. Richet, J.-P. Petitet, Coesite (SiO_2) as an extreme case of superheated crystal: an X-ray diffraction study up to 1776 K, Chem. Geol. 229 (2006) 57–63.
[63] V.M. Galkin, A.M. Dorochev, Yu V. Babitch, Termitcheskoe raschirenie koesita, Izvestia A.N. SSSR, Geochimia (1987) 1645–1646.
[64] B.J. Skinner, Thermal expansion of ten minerals, U. S. Geol. Surv. Res. Prof. Pap. 450-D. (1962) D109–D112.
[65] B.S. Hemingway, S.R. Bohlen, W.B. Hankins, E.F. Westrum Jr., O.L. Kuskov, Heat capacity and thermodynamic properties for coesite and jadeite, reexamination of the quartz-coesite equilibrium boundary, Am. Mineral. 83 (1998) 409–418.
[66] H.C. Helgeson, J. Delany, D.K. Bird, Summary and critique of the thermodynamic properties of rock-forming minerals, Am. J. Sci. 278A (1978) 1–229.
[67] K.R. Hosieni, R.A. Howald, M.W. Scanlon, Thermodynamics of the lambda transition and the equation of state of quartz, Am. Mineral. 70 (1985) 782–793.
[68] E. Salje, B. Wruck, S. Marais, Order parameter saturation at low temperatures – numerical results for displacive and O/D systems, Ferroelectrics 124 (1991) 185–188.
[69] R.G. Berman, T.H. Brown, Heat capacity of minerals in the system Na_2O-K_2OCaO-MgO-FeO-Fe_2O_3-Al_2O_3-SiO_2-TiO_2-H_2O-CO_2: representation, estimation, and high temperature extrapolation, Contrib. Mineral. Petrol. 89 (1985) 168–183.
[70] R.G. Berman, T.H. Brown T.H, Erratum. Heat capacity of minerals in the system Na_2O-K_2O-CaO-MgO-FeO-Fe_2O_3-Al_2O_3-SiO_2-TiO_2-H_2O-CO_2: representation, estimation, and high temperature extrapolation, Contrib. Mineral. Petrol. 94 (1986) 262.
[71] R.J. Ackermann, C.A. Sorrell, Thermal expansion and the high-low transformation in quartz. I. High-temperature X-ray studies, J. Appl. Cryst. 7 (1974) 461–467.
[72] E. Bourova, P. Richet, Quartz and cristobalite: high-temperature cell parameters and volumes of fusion, Geophys. Res. Lett. 25 (1998) 2333–2336.
[73] D. Taylor, Thermal expansion. IV. Binary oxides with the silica structures, Br. Ceram. Trans. J. 83 (1984) 129–134.
[74] W. Pies, A. Weiss, G. Will, Crystal structure data of inorganic compounds – Key element: Si. Part I, in: K.-H. Hellwege, A.M. Hellwege (Eds.), Landolt-Börnstein New Series – Group III Condensed Matter, Vol. 7D1a, Springer, Berlin.
[75] D.R. Hamann, Generalized gradient theory for silica phase transitions, Phys. Rev. Lett. 76 (1996) 660–663.
[76] S.N. Vaidya, S. Bailey, T. Pasternack, G.C. Kennedy, Compressibility of fifteen minerals to 45 kilobars, J. Geophys. Res. – Solid Earth 78 (1973) 6893–6898.
[77] B. Olinger, P.M. Halleck, The compression of a-quartz, J. Geophys. Res. – Solid Earth 81 (1976) 5711–5714.
[78] H. d'Amour, W. Denner, H. Schulz, Structure determination of a-quartz up to 68×10^8 Pa, Acta Cryst. B35 (1979) 550–555.
[79] L. Levien, C.T. Prewitt, D.L. Weidner, Structure and elastic properties of quartz at pressure, Am. Mineral. 65 (1980) 920–930.
[80] L. Cartz, J.D. Jorgensen, The high-pressure behavior of a-quartz, oxynitride, and nitride structures, J. Appl. Phys. 52 (1981) 236–244.
[81] J.D. Jorgensen, Compression mechanisms in a-quartz structures – SiO_2 and GeO_2, J. Appl. Phys. 49 (1978) 5473–5478.
[82] L.H. Cohen, W. Klement Jr., High-low quartz inversion: determination to 35 kilobars, J. Geophys. Res. – Solid Earth 72 (1967) 4245–4251.

[83] P.W. Mirwald, H.-J. Massonne, The low-high quartz and quartz-coesite transition to 40 kbar between 600° and 1600°C and some reconnaissance data on the effect of $NaAlO_2$ component on the low quartz–coesite transition, J. Geophys. Res. – Solid Earth 85 (1980) 6983–6990.
[84] R.T. Downs, D.C. Palmer, The pressure behavior of a cristobalite, Am. Mineral. 79 (1994) 9–14.
[85] D.M. Teter, G.V. Gibbs, M.B. Boisen Jr., D.C. Allan, M.P. Teter, First-principles study of several hypothetical silica framework structures, Phys. Rev. B 52 (1995) 8064–8073.
[86] I.P. Swainson, M.T. Dove, On the thermal expansion of b-cristobalite, Phys. Chem. Miner. 22 (1995) 61–65.
[87] L.H. Cohen, W. Klement Jr., High-low cristobalite transitions in SiO_2, $AlPO_4$ and $GaPO_4$: investigations by differential thermal analysis under hydrostatic pressures ≤ 6 kbar, Philos. Mag. 39A (1979) 399–404.
[88] A.B. Thompson, M. Wennemer, Heat capacities and inversions in tridymite, cristobalite and tridymite-cristobalite mixed phases, Am. Mineral. 64 (1979) 1018–1026.
[89] M.A. Mosesman, K.S. Pitzer, Thermodynamic properties of the crystalline forms of silica, J. Am. Chem. Soc. 63 (1941) 2348–2356.
[90] J.B. Austin, The coefficient of linear thermal expansion of tridymite, J. Am. Chem. Soc. 76 (1954) 6019–6020.
[91] L.H. Cohen, W. Klement Jr., Tridymite: effect of hydrostatic pressure to 6 kbars on temperatures of two rapidly reversible transitions, Contrib. Mineral. Petrol. 71 (1980) 401–405.
[92] U. Raz, Thermal and Volumetric Measurements on Quartz and Other Substances at Pressures up to 6 kbars and Temperatures up to 700°C. Ph.D Thesis, ETH Research Collection, doi: https://doi.org/10.3929/ethz-a-000306771.
[93] V. Dmitriev, V. Torgashev, P. Tolédano, E.K.H. Salje, Theory of SiO_2 polymorphs, Europhys. Lett. 37 (1997) 553–558.
[94] A.K. Chatterjee, High belite cements – present status and future technological options: part I, Cem. Concr. Res. 26 (1996) 1213–1225.
[95] H.F.W. Taylor, Cement Chemistry, second ed, Thomas Telford Publishing, London, 1997.
[96] A.A. Freitas, R.L. Santos, R. Colaço, R. Bayão Horta, J.N. Canongia Lopes, From lime to silica and alumina: systematic modeling of cement clinkers using a general force-field, Phys. Chem. Chem. Phys. 17 (2015) 18477–18494.
[97] C. Remy, D. Andrault, M. Madon, High-temperature, high-pressure X-ray investigation of dicalcium silicate, J. Am. Ceram. Soc. 80 (1997) 851–860.
[98] K. Niesel, The importance of the a'_L-a'_H, transition in the polymorphism of dicalcium silicate, Silic. Ind. 37 (1972) 136–138.
[99] R.G. Berman, T.H. Brown, A thermodynamic model for multicomponent melts, with application to the system CaO-Al_2O_3-SiO_2, Geochim. Cosmochim. Acta 48 (1984) 661–678.
[100] J.L. Haas, G.R. Robinson, B.S. Hemingway, Thermodynamic tabulations for selected phases in the system CaO-Al_2O_3-SiO_2-H_2O at 101.325 kPa (1 atm) between 273.15 and 1800 K, J. Phys. Che. Ref. Data 10 (1981) 575–669.
[101] H. Saalfeld, X-Ray investigation of single crystals of b-Ca_2SiO_4 (Larnite) at high temperatures, Am. Mineral. 60 (1975) 824–827.
[102] P. Barnes, C.H. Fentiman, J.W. Jeffery, Structurally related dicalcium silicate phases, Acta Cryst. A26 (1980) 353–356.
[103] J. Forest, Connaissance de l'orthosilicate de calcium, Bull. Soc. Fr. Minéral. Cristallogr. 94 (1971) 118–137.
[104] P. Richet, R.A. Robie, B.S. Hemingway, Thermodynamic properties of wollastonite, pseudowollastonite and $CaSiO_3$ glass and liquid, Eur. J. Mineral. 3 (1991) 475–484.
[105] I. Kushiro, Wollastonite-pseudowollastonite inversion, Carnegie. Inst. Wash. Yb. 63 (1964) 83–84.
[106] E.F. Osborn, The system $CaSiO_3$-diopside-anorthite, Am. J. Sci. 240 (1942) 751–788.
[107] K. Adamkovikova, L. Kosa, I. Proks, The heat of fusion of $CaSiO_3$, Silikaty 24 (1980) 193–201.
[108] E. Essene, High-pressure transformations in $CaSiO_3$, Contrib. Mineral. Petrol. 45 (1974) 247–250.
[109] W. Joswig, E.F. Paulus, B. Winkler, V. Milman, The crystal structure of $CaSiO_3$walstromite, a special isomorph of wollastonite-II, Z. Krist. 218 (2003) 811–818.
[110] K.M. Krupka, R.A. Robie, B.S. Hemingway, D.M. Kerrick, J. Ito, Low-temperature heat capacities and derived thermodynamic properties of anthophyllite, diopside, enstatite, bronzite and wollastonite, Am. Mineral. 70 (1985) 249–260.
[111] K.M. Krupka, R.A. Robie, B.S. Hemingway, D.M. Kerrick, High-temperature heat capacities and derived thermodynamic properties of anthophyllite, diopside, dolomite, enstatite, bronzite, talc, tremolite, and wollastonite, Am. Mineral. 70 (1985) 261–271.
[112] W.P. White, Silicate specific heats, Am. J. Sci. 47 (1919) 1–214.
[113] V.H. Wagner, Zur thermochemie der metalsilikate des calciums und magnesiums und des diopsids, Z. Anorg. Allg. Chem. 208 (1932) 1–22.
[114] H. Elsner von Gronow, H.E. Schwiete, Die spezifischen wärmen fon CaO, Al_2O_3, CaO-Al_2O_3, $3CaO$-Al_2O_3, $2CaO$-SiO_2, $3CaO$-SiO_2, $2CaO$-Al_2O_3-SiO_2 von 20 bis 1500 °C, Z. Anorg. Allg. Chem. 216 (1933) 185–195.
[115] V. Swamy, L.S. Dubrovinsky, Thermodynamic data for the phases in the $CaSiO_3$ system, Geochim. Cosmochim. Acta 61 (1997) 1181–1191.
[116] N.D. Chatterjee, W. Johannes, H. Leistner, The system CaO-Al_2O_3-SiO_2-H_2O: new phase equilibria data, some calculated phase relations, and their petrological applications, Contrib. Mineral. Petrol. 88 (1984) 1–13.
[117] Y. Wang, D.J. Weidner, F. Guyot, Thermal equation of state of $CaSiO_3$ perovskite, J. Geophys. Res. – Solid Earth 101 (1996) 661–672.
[118] K.K. Kelley, Heats and Free Energies of Formation of Anhydrous Silicates, U.S. Department of the Interior – Bureau of Mines, Washington, 1962, pp. 4–7 U.S.

Bur. Mines Rep. Invest. 5901.
[119] K.K. Kelley, E.G. King, (U.S. Bur. Mines Bull)Contributions to the Data on Theoretical Metallurgy. XIV. Entropies of the Elements and Inorganic Compounds 592, U.S. Department of the Interior – Bureau of Mines, Washington, 1961.
[120] E.G. King, Heats of formation of crystalline calcium orthosilicate, tricalcium silicate and zinc orthosilicate, J. Am. Chem. Soc. 73 (1951) 653–658.
[121] B.J. Skinner, Thermal expansion, in: S.P. ClarkJr. (Ed.), Handbook of Physical Constants 97, Geological Society of America Memoirs, Boulder, CO, 1966, pp. 75–95.
[122] P.J. Spencer, The Thermodynamic Properties of Silicates (NPL Rept. Chem. 21), National Physical Laboratory, Teddington, UK, 1973.
[123] W.F. Weeks, A thermochemical study of equilibrium relations during metamorphism of siliceous carbonate rocks, J. Geol. 64 (1956) 245–270.
[124] T.J.B. Holland, R. Powell, An internally consistent thermodynamic dataset for phases of petrological interest, J. Metamorph. Geol. 16 (1998) 309–343.
[125] T. Gasparik, K. Wolf, C.M. Smith, Experimental determination of phase relations in the $CaSiO_3$ system from 8 to 15 GPa, Am. Mineral. 79 (1994) 1219–1222.
[126] R.J. Angel, N.L. Ross, F. Seifert, T.F. Fliervoet, Structural characterization of pentacoordinate silicon in a calcium silicate, Nature 384 (1996) 441–444.
[127] R.J. Angel, Transformation of fivefold-coordinated silicon to octahedral silicon in calcium silicate, $CaSi_2O_5$, Am. Mineral. 82 (1997) 836-834.
[128] R.J. Angel, M. Kunz, R. Miletich, A.B. Woodland, M. Koch, R.L. Knoche, Effect of isovalent Si,Ti substitution on the bulk moduli of $Ca(Ti_{1-x}Si_x)SiO_5$ titanites, Am. Mineral. 84 (1999) 282–287.
[129] Y.G. Yu, R.J. Angel, N.L. Ross, G.V. Gibbs, Pressure impact on the structure, elasticity, and electron density distribution of $CaSi_2O_5$, Phys. Rev. B 87 (2013) 184112.
[130] M. Schoenitz, A. Navrotsky, N. Ross, Enthalpy of formation of $CaSi_2O_5$, a quenched high-pressure phase with pentacoordinate silicon, Phys. Chem. Miner. 28 (2001) 57–60.
[131] M. Akaogi, M. Yano, Y. Tejima, M. Iijima, H. Kojitani, High-pressure transitions of diopside and wollastonite: phase equilibria and thermochemistry of $CaMgSi_2O_6$, $CaSiO_3$ and $CaSi_2O_5$-$CaTiSiO_5$ system, Phys. Earth Planet. Int. 143–144 (2004) 145–156.
[132] M. Kanzaki, J.F. Stebbins, X. Xue, Characterization of quenched high pressure phases in $CaSiO_3$ system by XRD and ^{29}Si NMR, Geophys. Res. Lett. 18 (1991) 463–466.
[133] G. Ottonello, Thermodynamic constraints arising from the polymeric approach to silicate slags: the system CaO-FeO-SiO_2 as an example, J. Non-Cryst. Solids 282 (2001) 72–85.
[134] G. Ottonello, Chemical interactions and configurational disorder in silicate melts, Ann. Geophys. 48 (2005) 561–581.
[135] G.W. Toop, C.S. Samis, Some new ionic concepts of silicate slags, Can. Metall. Quart. 1 (1962) 129–152.
[136] G.W. Toop, C.S. Samis, Activities of ions in silicate melts, Trans. Met. Soc. AIME 224 (1962) 878–887.
[137] P. Richet, G. Ottonello, The Earth as a multiscale quantum-mechanical system, Comptes Rend. Geosci. 346 (2014) 317–325.
[138] C.L. Fenner, The stability relations of the silica minerals, Am. J. Sci. 36 (1913) 331–384.
[139] G.C. Kennedy, G.J. Wasserburg, H.C. Heard, R.C. Newton, The upper three phase region in the system SiO_2-H_2O, Am. J. Sci. 260 (1962) 501–521.
[140] I.A. Ostrovsky, PT-diagram of the system SiO_2-H_2O, Geol. J. 5 (1966) 127–134.
[141] P.E. Grattan-Bellew, Quartz-tridymite transition under hydrothermal conditions, Exp. Miner. 11 (1978) 128–139.
[142] I. Jackson, Melting of the silica isotypes SiO_2, BeF_2 and GeO_2 at elevated pressures, Phys. Earth Planet. Int. 13 (1976) 218–231.
[143] P. Hudon, I.-H. Jung, D.R. Baker, Experimental investigation and optimization of thermodynamic properties and phase diagrams in the systems CaO-SiO_2, $MgOSiO_2$, $CaMgSi_2O_6$-SiO_2 $CaMgSi_2O_6$-Mg_2SiO_4 to 1.0 GPa, J. Petrol. 46 (2005) 1859–1880.
[144] S.R. Bohlen, L. Boettcher, The quartz ↔ coesite transformation: a precise determination and the effects of other components, J. Geophys. Res. – Solid Earth 87 (1982) 7073–7078.
[145] K. Bose, J. Ganguly, Quartz-coesite transition revisited: reversed experimental determination at 500–1200 °C and retrieved thermochemical properties, Am. Mineral. 80 (1995) 231–238.
[146] M. Kanzaki, Melting of silica up to 7 GPa, J. Am. Ceram. Soc. 73 (1990) 3706–3707.
[147] J. Zhang, R.C. Liebermann, T. Gasparik, C.T. Herzberg, Melting and subsolidus relations of SiO_2 at 9–14 GPa, J. Geophys. Res. – Solid Earth 98 (1993) 19785–19793.
[148] J. Zhang, B. Li, W. Utsumi, R.C. Liebermann, In situ X-ray observations of the coesite-stishovite transition: reversed phase boundary and kinetics, Phys. Chem. Miner. 23 (1996) 1–10.
[149] C. Remy, F. Guyot, M. Madon, High pressure polymorphism of dicalcium silicate Ca_2SiO_4. A transmission electron microscopy study, Phys. Chem. Miner. 22 (1995) 419–427.

[150] Y. Wang, D.J. Weidner, Thermoelasticity of $CaSiO_3$ perovskite and implications for the lower mantle, Geophys. Res. Lett. 21 (1994) 895–898.

[151] Z. Xiong, X. Liu, S.R. Shieh, S. Wang, L. Chang, J. Tang, X. Hong, Z. Zhang, H. Wang, H. Some, thermodynamic properties of larnite (b-Ca_2SiO_4) constrained by high T/P experiment and/or theoretical simulation, Am. Mineral. 101 (2016) 277–288.

[152] E.F. Osborn, J.F. Schairer, The ternary system pseudo-wollastonite–akermanite– gehlenite, Am. J. Sci. 239 (1941) 715–763.

[153] H.G. Huckenholz, H.S. Yoder Jr., The gehlenite-H_2O and wollastonite-H_2O systems, Carnegie. Inst. Wash. Yb. 73 (1974) 440–443.

[154] W.-L. Huang, P.J. Wyllie, Melting and subsolidus melting relationships for $CaSiO_3$ to 35 kilobars pressure, Am. Mineral. 60 (1975) 213–217.

[155] Y. Sueda, T. Irifune, A. Yamada, T. Inoue, X. Liu, K. Funakoshi, The phase boundary between $CaSiO_3$ perovskite and Ca_2SiO_4 + $CaSi_2O_5$ determined by in situ X-ray observations, Geophys. Res. Lett. 33 (2006) L10307.

[156] E.F. Osborn, The compound merwinite ($3CaO{\cdot}MgO{\cdot}2SiO_2$) and its stability relations within the system CaO-MgO-SiO_2 (preliminary report), J. Am. Ceram.
Soc. 26 (1943) 321–332.

[157] J.H. Welch, W. Gutt, Tricalcium silicate and its stability within the system $CaOSiO_2$, J. Am. Ceram. Soc. 42 (1959) 11–15.

[158] W. Gutt, Manufacture of Portland cement from phosphate raw materials -
Building Research Station Paper CP90/68, Publications Officer, London, 1968.

[159] G.A. Rankin, F.E. Wright, The ternary system CaO-Al_2O_3-SiO_2, Am. J. Sci. 39 (1915) 1–79.

[160] M. Hillert, B. Sundman, X. Wang, T. Barry, A reevaluation of the rankinite phase in the CaO-SiO_2 system, CALPHAD 15 (1991) 53–58.

[161] J. Zawadzki, J. Gotlieb, Decomposition of alite, Bull. Int. Acad. Pol. Sci., Cl. Sci.
Math. Nat. A1940–1946 (1948) 32–34.

[162] E.S. Sheperd, G.A. Rankin, F.E. Wright, Preliminary report on the ternary system CaO-Al_2O_3-SiO_2, J. Ind. Eng. Chem. 3 (1911) 211–227.

[163] F.P. Glasser, E.F. Osborn, Phase equilibrium studies in the system CaO-$Cr_2O_3SiO_2$, J. Am. Ceram. Soc. 41 (1958) 358–367.

[164] G. Troemel, W. Fix, R. Heinke, Tonind Ztg, Keram. Rundsch. 93 (1969) 1–8.

[165] H. Mao, M. Hillert, M. Selleby, B. Sundman, Thermodynamic assessment of the CaO-Al_2O_3-SiO_2 system, J. Am. Ceram. Soc. 89 (2006) 298–308.

[166] W. Huang, M. Hillert, X. Wang, Thermodynamic assessment of the CaO-$MgOSiO_2$ system, Metall. Mat. Trans. 26A (1995) 2293–2310.

[167] D.D. Wagman, W.H. Evans, V.B. Parker, R.H. Schumm, I. Halow, S.M. Bailey, K. L. Churney, R.L. Nuttall R.L, The NBS tables of chemical thermodynamic properties. Selected values for inorganic and $_C1$ and $_C2$ organic substances in SI units, Journal of Physical and Chemical Reference Data, Volume 11, Supplement No. 2, American Chemical Society and American Institute of Physics for the National Bureau of Standards, Washington, D.C, 1982.

[168] M. Blander, A.D. Pelton, Computer-assisted Analyses of the Thermodynamic Properties of Slags in Coal-combustion Systems, Argonne National Laboratory Technical Report ANL/FE-83-19, Argonne, Illinois, 1983.

[169] J.D. Tewhey, P.C. Hess, The two phase region in the CaO-SiO_2 system: experimental data and thermodynamic analysis, Phys. Chem. Glass. 20 (1979) 41–53.

[170] V.B.M. Hageman, G.J.K. van den Berg, H.J. Janssen, H.A.J. Oonk, A reinvestigation of liquid immiscibility in the SiO_2-CaO system, Phys. Chem. Glass. 27 (1986) 100–106.

[171] J.V. Greig, Immiscibility in silicate melts, Am. J. Sci. 13 (1927) 1–44.

[172] F.C. Kracek, The cristobalite liquidus in the alkali oxide-silica systems and the heat of fusion of cristobalite, J. Am. Chem. Soc. 52 (1930) 1436–1442.

[173] Y.I. Ol'shanskii, Equilibrium of two immiscible liquids in silicate systems of alkaliearth metals, Dokl. Acad. Nauk. USSR 76 (1951) 93–96.

[174] A.B. Thompson, M. Aerts, A.C. Hack, Liquid immiscibility in silicate melts and related systems, in: A. Liebscher, C.A. Heinrich (Eds.), , Fluid-Fluid Interactions, Reviews in Mineralogy & Geochemistry 65, Mineralogical Society of America, Chantilly, 2007, pp. 99–127.

[175] P. Hudon, I.-H. Jung, D.R. Baker, Effect of pressure on liquid-liquid miscibility gaps: a case study of the systems CaO-SiO_2, MgO-SiO_2, and $CaMgSi_2O_6$-SiO_2, J. Geophys. Res. – Solid Earth 109 (2004) B03207.